ARTICLE IN PRESS

Available online at www.sciencedirect.com
SCIENCE DIRECT®

Journal of Computational Physics xxx (2004) xxx–xxx

JOURNAL OF COMPUTATIONAL PHYSICS

www.elsevier.com/locate/jcp

Balanced finite volume WENO and central WENO schemes for the shallow water and the open-channel flow equations

Nelida Črnjarić-Žic *, Senka Vuković, Luka Sopta

Faculty of Engineering, University of Rijeka, Vukovarska 58, 51000 Rijeka, Croatia

Received 25 September 2003; received in revised form 20 April 2004; accepted 21 April 2004

Abstract

The goal of this work is to extend finite volume WENO and central WENO schemes to the hyperbolic balance laws with geometrical source term and spatially variable flux function. In particular, we apply proposed schemes to the shallow water and the open-channel flow equations where the source term depends on the channel geometry. For obtaining stable numerical schemes that are free of spurious oscillations, it becomes crucial to use the decomposed source term evaluation, which maintains the balancing between the flux gradient and the source term. In addition, the open-channel flow equations contain spatially variable flux function. The appropriate definitions of the terms that arise in the source term decomposition, in combination with the Roe approximate Riemann solver that includes the spatial derivative of the flux function, lead to the finite volume WENO scheme that satisfies the exact conservation property – the property of preserving the quiescent flow exactly. When the central WENO schemes are applied, additional reformulations are introduced for the transition from the staggered values to the nonstaggered ones and vice versa by using the WENO reconstruction procedure. The proposed central WENO schemes also preserve the quiescent flow, but only in prismatic channels. In various test problems the obtained balanced schemes show improvements in comparison with the standard versions of the proposed type schemes, as well as with some other first- and second-order numerical schemes.

AMS: 65M06; 76M20; 35L65

Keywords: Finite volume WENO schemes; Central WENO schemes; Shallow water equations; Open-channel flow equations; Balanced scheme; Exact conservation property; Hyperbolic balance law

1. Introduction

We consider the one-dimensional hyperbolic balance law system

$$\partial_t \mathbf{u} + \partial_x \mathbf{f}(\mathbf{u}, x) = \mathbf{g}(\mathbf{u}, x). \tag{1}$$

* Corresponding author.
E-mail addresses: nelida@riteh.hr (N. Črnjarić-Žic), senka.vukovic@ri.hinet.hr (S. Vuković), luka.sopta@riteh.hr (L. Sopta).

0021-9991/$ - see front matter
doi:10.1016/j.jcp.2004.04.012

Here, $\mathbf{u}$ is the vector variable, $\mathbf{f}(\mathbf{u},x)$ is the flux, and $\mathbf{g}(\mathbf{u},x)$ is the source term. The goal of this work is to extend finite volume WENO and central WENO schemes to the hyperbolic balance laws of type (1), where $\mathbf{f}(\mathbf{u},x)$ is a spatially variable flux function and $\mathbf{g}(\mathbf{u},x)$ is a geometrical source term. In particular, we apply proposed algorithms to the shallow water equations and the open-channel flow equations. In these balance law systems the source term depends on the geometry of the channel, hence it is of the geometrical type. In addition, in the open-channel flow equations, the flux is spatially dependent.

In the last few years various papers were published that were concentrated on the numerical approximations for balance laws. The most important property in connection with the numerical schemes that should be able to treat correctly the shallow water equations was given by Bermùdez and Vázquez [2]. They introduced the notion of the exact conservation property for the numerical schemes that preserve the quiescent flow exactly. The first-order finite volume scheme they developed for the shallow water equations used a decomposed approximation of the source term. Based on that approach Hubbard and García-Navarro [9] extended the second-order finite volume scheme, flux-limited and MUSCL scheme, to the shallow water equations. Other first- and second-order schemes that were applied to the shallow water equations and that used the idea of balancing between the source term and the flux gradient were: wave propagation algorithm by LeVeque [18], gas-kinetic scheme by Xu [27], kinetic-scheme by Perthame and Simeoni, central-upwind schemes given by Kurganov and Levy [16], a family of numerical flux-splitted solvers proposed in [5,6], etc. The surface gradient method in combination with the second-order finite volume scheme that also lead to the scheme that satisfies the exact conservation property was proposed in [33]. By combining the well-balanced schemes that were initially introduced by Greenberg and LeRoux in the scalar case [14] and later by Gosse for the balance laws systems [12], with some approximate Riemann solvers, Gallouët et al. [10] developed the numerical schemes for computation of the shallow water equations with topography, which can preserve the steady-state solutions. First higher-order schemes that respect balancing between the source term and the flux gradient, which is crucial for preserving some steady-state solutions were developed in [29]. In that work we extended the finite difference ENO and WENO schemes to the shallow water equations. Since in the finite difference version of the ENO and WENO schemes the numerical flux is obtained by the WENO reconstruction, which is applied to the flux function directly, to achieve balancing the source term approximation must have the similar form. Therefore, the decomposed approximation of the source term was extended with the higher-order terms necessary for obtaining balancing. Also, some additional reformulations of the WENO reconstruction procedure that lead to the balanced ENO and WENO schemes were introduced. We also extended the same schemes in [7] for the sediment transport equations such that the exact conservation property is achieved. The difference in sediment transport equations when compared to the shallow water equations lies in the fact that a nonconservative product arises in that balance law instead of the geometrical source term.

All the mentioned papers studied the way to treat the terms arising from the bed level changes. However, when the open-channel flow equations are considered, a second part of the source term that includes the changes in the cross-section of the channel arises. The correct numerical approximation of that part of the source term is crucial for obtaining the balanced numerical scheme. Moreover, the spatially varied flux is present, hence the spatial part of the flux must be incorporated into its numerical approximation. In [30], we developed upwind, first- and second-order finite volume schemes with the exact conservation property for the open-channel flow equations with the arbitrary cross-section channel. Similar results, based on different formulations of the flux and the source term, were given by García-Navarro and Vázquez-Cendon [11]. Hubbard and García-Navarro [9] also considered the open-channel flow equations, but their discussion was reduced only to the channels with the rectangular cross-sections. The continuation of the work presented in [30] was connected with the extension of the finite difference ENO and WENO schemes to the balanced laws with spatially varying flux [31], where these schemes were applied to the open-channel flow equations and to the one-dimensional elastic wave equations. For both

balance laws, the exact conservation property for some steady-state solution was satisfied. In [1], the extension of the wave propagation algorithm to the hyperbolic conservation and balance laws with spatially varying flux functions was considered.

In this work we consider the finite volume WENO schemes that were originally introduced by Liu et al. [22]. The crucial difference from the finite difference WENO schemes lies in the fact that the WENO reconstruction procedure is applied to the solution and not to the flux function values (see [8,24]). As a consequence of that, the finite volume WENO schemes can be applied to the nonuniform mesh. Moreover, in the finite difference WENO schemes, for obtaining balancing, the WENO reconstruction must be applied to the source term values, while in the finite volume case the source term should be appropriately discretized at the states that are obtained with the WENO reconstruction. The balancing procedure is actually connected with the numerical flux function that is used on the obtained reconstructed values. We consider here the case when the Roe approximate Riemann solver is used. In the extension of the finite volume WENO schemes to the balance laws, we apply two main ideas. The first one is connected with the source term approximation that is done in the similar way as it was proposed by Hubbard and García-Navarro [9] for the MUSCL schemes. The second one is to include the spatial derivative of the flux into its numerical approximation. A similar numerical treatment we proposed in [30] for the first- and second-order upwind schemes.

The central WENO schemes for the hyperbolic conservation laws were developed by Levy et al. [20]. Higher-order central WENO schemes were considered in [23]. Their construction was based on using the staggered grid. In [15], the first- and the second-order nonstaggered central schemes were developed. By applying the similar approach to the central WENO schemes, we obtain the nonstaggered central WENO schemes, which we consider here. The goal is to extend mentioned schemes to the shallow water and to the open-channel flow equations such that the quiescent flow is preserved.

The organization of the paper is as follows. In Section 2, we present the general formulation of the new finite volume WENO schemes. The numerical approximations for the spatially varied flux and for the source term are defined such that the balancing between the flux gradient and the source term can be obtained. Of course, the exact definitions of those terms depend on the particular balance law system and we give them in the Section 4 for the open-channel flow equations and for the shallow water equations as a special case of the open-channel flow equations. We prove that the proposed scheme satisfies the exact conservation property. In Section 3, the general formulation of the extended nonstaggered central WENO scheme for balance laws is presented. We again determine the undefined terms in Section 4. Moreover, we introduce some reformulations of the algorithm of the transition from the staggered values to the nonstaggered ones and then back. These reformulations are based on the quiescent flow steady state we want to be preserved. What we must emphasize is the fact that unlike for the finite volume WENO, the balancing for the central WENO scheme could not be obtained for arbitrary channels, but only for rectangular cross-section channels with the algorithm we propose in this paper. Namely, in the general case it is not clear how the transformations between the staggered and the nonstaggered mesh have to be made, such that the steady quiescent flow state is preserved. Finally, with the numerical results in Section 5, we illustrate the improvement of the proposed approach for both considered schemes. First, we present the tests for the shallow-water equations and then the more general open-channel flow test cases. The accuracy test results show that with the proposed reformulations the spatial order of accuracy of our schemes is not deteriorated.

2. Finite volume WENO schemes for balance laws

In order to solve the balance law system (1) with the finite volume WENO type scheme, we rewrite it first in the form

$$\partial_t \mathbf{u} = -\partial_x \mathbf{f}(\mathbf{u}, x) + \mathbf{g}(\mathbf{u}, x). \tag{2}$$

Let us consider the semi-discrete formulation of the scheme. For that purpose we introduce a spatial discretization of the considered domain with cells $I_i = [x_{i-\frac{1}{2}}, x_{i+\frac{1}{2}}]$, $i = 1, \ldots, N$. We denote the ith cell size with Δx_i and the cell center $x_i = \frac{1}{2}(x_{i-\frac{1}{2}} + x_{i+\frac{1}{2}})$.

Let $\overline{\mathbf{u}}_i(t)$ denote the cell average of $\mathbf{u}(\cdot, t)$ over the cell I_i, i.e.,

$$\overline{\mathbf{u}}_i(t) = \frac{1}{\Delta x_i} \int_{x_{i-\frac{1}{2}}}^{x_{i+\frac{1}{2}}} \mathbf{u}(x, t)\, \mathrm{d}x. \tag{3}$$

Then, an equivalent formulation for (2) over the ith cell in terms of cell averages reads

$$\frac{\mathrm{d}\overline{\mathbf{u}}_i(t)}{\mathrm{d}t} = -\frac{1}{\Delta x_i}\left(\mathbf{f}(\mathbf{u}(x_{i+\frac{1}{2}}, t), x_{i+\frac{1}{2}}) - \mathbf{f}(\mathbf{u}(x_{i-\frac{1}{2}}, t), x_{i-\frac{1}{2}})\right) + \frac{1}{\Delta x_i} \int_{x_{i-\frac{1}{2}}}^{x_{i+\frac{1}{2}}} \mathbf{g}(\mathbf{u}(x, t), x)\, \mathrm{d}x. \tag{4}$$

The discretization process consists of two parts. First, the time discretization of the left-hand side of (4) is done by using a classical TVD Runge–Kutta method and second, for the discretization of the right-hand side of (4) the finite volume WENO reconstruction is applied. Since the classical finite volume WENO scheme considers just the homogeneous hyperbolic conservation law system, we develop here its extension to the balance law with geometrical source term and with an additional extension to the spatially varied flux function. For a detailed review of the standard WENO schemes we refer to the papers [8,25] and the lecture notes [24].

The numerical approximation of the right-hand side of (4) we denote by $\mathbf{L}_i$,

$$\mathbf{L}_i = -\frac{1}{\Delta x_i}(\mathbf{f}_{i+\frac{1}{2}} - \mathbf{f}_{i-\frac{1}{2}}) + \frac{1}{\Delta x_i}\mathbf{G}_i. \tag{5}$$

Here, the numerical flux $\mathbf{f}_{i+\frac{1}{2}}$ represents the approximation for the term $\mathbf{f}(\mathbf{u}(x_{i+\frac{1}{2}}, t), x_{i+\frac{1}{2}})$, while $\mathbf{G}_i$ stands for the numerical approximation to the integral of the source term over the cell I_i. The numerical flux is evaluated by using an exact or approximate Riemann solver, i.e.,

$$\mathbf{f}_{i+\frac{1}{2}} = \mathbf{F}(\mathbf{u}^-_{i+\frac{1}{2}}, \mathbf{u}^+_{i+\frac{1}{2}}) \tag{6}$$

for the monotone numerical flux function $\mathbf{F}$, which satisfies some requirements that are, for example, given in [24]. The values $\mathbf{u}^-_{i+\frac{1}{2}}$ and $\mathbf{u}^+_{i+\frac{1}{2}}$ are high-order pointwise approximation to the solution $\mathbf{u}$ at the $(i+\frac{1}{2})$th cell boundary obtained from the known cell averages $\overline{\mathbf{u}}_i(t)$, $i = 1, \ldots, N$ by using the WENO reconstruction procedure.

We present here just the final expression of this reconstruction for any function v. Let us suppose the cell average values $\overline{v}_i$ of that function are known. Then, the $(2r-1)$th-order WENO approximations $v^{\pm}_{i+\frac{1}{2}}$ on the $(i+\frac{1}{2})$th cell boundary can be computed as

$$v^{\pm}_{i+\frac{1}{2}} = \sum_{s=s^{\pm}_{\min}}^{s^{\pm}_{\max}} \sum_{j=0}^{r-1} \omega_{r,s}(v)\, a^{\pm}_{r,s,j}\, \overline{v}_{i-r+1+s+j}. \tag{7}$$

Here, $s^-_{\min} = 0$, $s^-_{\max} = r-1$, $s^+_{\min} = 1$ and $s^+_{\max} = r$. The coefficients $a^{\pm}_{r,s,j}$, $j = 0, \ldots, r-1, s = s^{\pm}_{\min}, \ldots, s^{\pm}_{\max}$ depend on s, r and cell sizes Δx_i, and not on the values $\overline{v}_i$. On the uniform mesh their values become independent on the cell sizes, and can be, for example, found in [24]. Furthermore, $\omega_{r,s}(v)$, $s = s^{\pm}_{\min}, \ldots, s^{\pm}_{\max}$ are the nonlinear weights which depend on the local smoothness of the function v over the stencil $S_{r,s} = \{x_{i-r+1+s}, \ldots, x_{i+s}\}$, $s = s^{\pm}_{\min}, \ldots, s^{\pm}_{\max}$. In this way all the candidate stencils $S_{r,s}$ are included in this

WENO reconstruction, which becomes, with the correct choices of the coefficients, $(2r-1)$th-order accurate.

There are two possible choices of the WENO reconstruction for the variable $\mathbf{u}$: the componentwise and the characteristicwise reconstruction. In the first case the reconstruction is made for each component of the variable $\mathbf{u}$ separately, while in the second one the variable is first transformed into local characteristic fields where the WENO reconstruction is made, and then transformed back into physical space (see [24] for details).

After the values $\mathbf{u}^{\pm}_{i+\frac{1}{2}}$ are determined, the approximate Riemann solver has to be applied. In this work the Roe solver is used, therefore first the Roe average state has to be defined.

Suppose we have to find the Roe average $\widetilde{\mathbf{u}}_{\mathrm{Roe}}(\mathbf{u}',\mathbf{u}'')$ of the states $\mathbf{u}'$ and $\mathbf{u}''$ that are positioned at x' and x'', respectively. Since we consider the systems where the flux is spatially varying, if we denote the Jacobian matrix of the flux with $\mathbf{A}$ and the spatial derivative of the flux with $\mathbf{v}$, i.e., $\mathbf{v}=\partial\mathbf{f}/\partial x$, we have $\mathrm{d}\mathbf{f}=\mathbf{A}\,\mathrm{d}\mathbf{u}+\mathbf{v}\,\mathrm{d}x$. Thus, it is natural to define the extended Roe average state $\widetilde{\mathbf{u}}_{\mathrm{Roe}}(\mathbf{u}',\mathbf{u}'')$ as the state in which the following relation must hold:

$$\mathbf{f}''-\mathbf{f}'=\mathbf{A}(\widetilde{\mathbf{u}}_{\mathrm{Roe}}(\mathbf{u}',\mathbf{u}''))(\mathbf{u}''-\mathbf{u}')+\mathbf{V}(\mathbf{u}',\mathbf{u}'',x',x''). \tag{8}$$

In the above expression, the notations $\mathbf{f}'$ and $\mathbf{f}''$ are used for the values $\mathbf{f}(\mathbf{u}',x')$ and $\mathbf{f}(\mathbf{u}'',x'')$, respectively. $\mathbf{A}(\widetilde{\mathbf{u}}_{\mathrm{Roe}}(\mathbf{u}',\mathbf{u}''))$ is the value of the Jacobian matrix at the extended Roe average state, while the term $\mathbf{V}(\mathbf{u}',\mathbf{u}'',x',x'')$ stands for the numerical approximation of $\mathbf{v}\,\mathrm{d}x$. The expressions for $\widetilde{\mathbf{u}}_{\mathrm{Roe}}(\mathbf{u}',\mathbf{u}'')$ and $\mathbf{V}(\mathbf{u}',\mathbf{u}'',x',x'')$ depend on the particular balance law, so we will compute them later.

Now the Roe approximate Riemann solver can be presented. As defined in [9], for the spatially varying flux function it is given with

$$\mathbf{F}\left(\mathbf{u}^{-}_{i+\frac{1}{2}},\mathbf{u}^{+}_{i+\frac{1}{2}}\right)=\tfrac{1}{2}\left(\mathbf{f}^{-}_{i+\frac{1}{2}}+\mathbf{f}^{+}_{i+\frac{1}{2}}\right)-\tfrac{1}{2}\mathbf{R}_{i+\frac{1}{2}}|\Lambda_{i+\frac{1}{2}}|\mathbf{L}_{i+\frac{1}{2}}\left(\mathbf{u}^{+}_{i+\frac{1}{2}}-\mathbf{u}^{-}_{i+\frac{1}{2}}\right)-\tfrac{1}{2}\mathbf{R}_{i+\frac{1}{2}}\Lambda^{-1}_{i+\frac{1}{2}}|\Lambda_{i+\frac{1}{2}}|\mathbf{L}_{i+\frac{1}{2}}\mathbf{V}_{i+\frac{1}{2}}. \tag{9}$$

Here, $\mathbf{f}^{\pm}_{i+\frac{1}{2}}=\mathbf{f}(\mathbf{u}^{\pm}_{i+\frac{1}{2}},x_{i+\frac{1}{2}})$; $\mathbf{L}_{i+\frac{1}{2}}$, $\mathbf{R}_{i+\frac{1}{2}}$ and $\Lambda_{i+\frac{1}{2}}$ are matrices of the left eigenvectors, right eigenvectors and the diagonalized matrix of the eigenvalues, respectively, which belong to the numerical approximation of the Jacobian matrix $\mathbf{A}(\widetilde{\mathbf{u}}_{i+\frac{1}{2}})$ at the Roe average $\widetilde{\mathbf{u}}_{i+\frac{1}{2}}=\widetilde{\mathbf{u}}_{\mathrm{Roe}}(\mathbf{u}^{-}_{i+\frac{1}{2}},\mathbf{u}^{+}_{i+\frac{1}{2}})$. The abbreviation $\mathbf{V}_{i+\frac{1}{2}}$ is used for the term $\mathbf{V}(\mathbf{u}^{-}_{i+\frac{1}{2}},\mathbf{u}^{+}_{i+\frac{1}{2}},x_i,x_{i+1})$.

It remains to define the term $\mathbf{G}_i$. As the pointwise treatment does not work well when the source term is of the geometrical type, we apply here the idea of the source term decomposition (Fig. 1) and following [9] we use the expression

$$\mathbf{G}_i=\mathbf{G}_{i-\frac{1}{2},\mathrm{R}}+\mathbf{G}_{i+\frac{1}{2},\mathrm{L}}+\mathbf{G}_{i,\mathrm{C}}. \tag{10}$$

The first two terms in the above expression include the source term upwinding and are defined with

$$\mathbf{G}_{i+\frac{1}{2},\mathrm{L}}=\tfrac{1}{2}\left(I-\mathbf{R}_{i+\frac{1}{2}}\Lambda^{-1}_{i+\frac{1}{2}}|\Lambda_{i+\frac{1}{2}}|\mathbf{L}_{i+\frac{1}{2}}\right)\mathbf{G}_{i+\frac{1}{2}} \tag{11}$$

and

$$\mathbf{G}_{i+\frac{1}{2},\mathrm{R}}=\tfrac{1}{2}\left(I+\mathbf{R}_{i+\frac{1}{2}}\Lambda^{-1}_{i+\frac{1}{2}}|\Lambda_{i+\frac{1}{2}}|\mathbf{L}_{i+\frac{1}{2}}\right)\mathbf{G}_{i+\frac{1}{2}}. \tag{12}$$

The terms $\mathbf{G}_{i+\frac{1}{2}}=\mathbf{G}(\mathbf{u}^{-}_{i+\frac{1}{2}},\mathbf{u}^{+}_{i+\frac{1}{2}})$ and $\mathbf{G}_{i,\mathrm{C}}=\mathbf{G}(\mathbf{u}^{+}_{i-\frac{1}{2}},\mathbf{u}^{-}_{i+\frac{1}{2}})$, which are the approximations to the integrals of the source term, should be determined when the particular balance law is considered. Their definition is crucial for obtaining the balanced numerical scheme, i.e., the scheme that preserves some steady-state solutions as will be described in the proceeding of this paper.

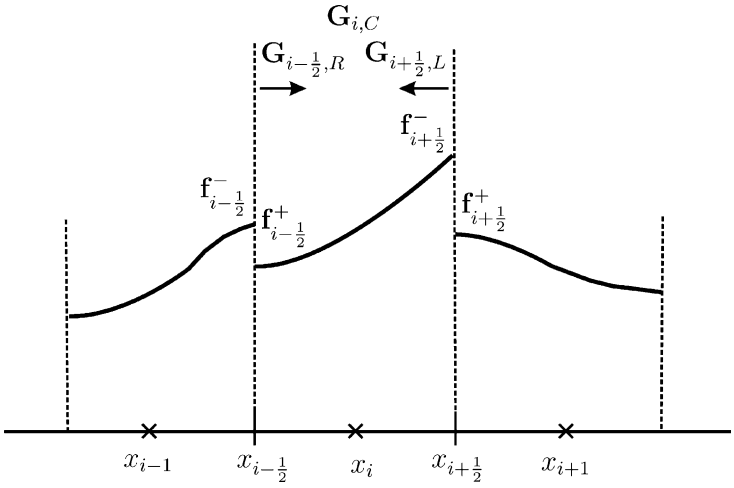

Fig. 1. Numerical flux and source terms for the finite volume WENO scheme.

The general formulation of the finite volume WENO scheme that we use in this paper can be concluded now. However, we are left with the need for the appropriate definitions of the extended Roe average $\widetilde{\mathbf{u}}_{i+\frac{1}{2}}$, the term $\mathbf{V}_{i+\frac{1}{2}}$, and the approximations to the integrals of the source term $\mathbf{G}_{i+\frac{1}{2}}$ and $\mathbf{G}_{i,C}$.

At the end we refer to the order of accuracy of the considered schemes. Since we expect that the order of accuracy is not deteriorated with the proposed extensions, the finite volume WENO scheme, which uses the r points stencils should be $(2r-1)$th-order accurate.

3. Central WENO schemes for balance laws

In this section we give a short overview of the central WENO schemes with the extension to the balance laws. More detailed descriptions of the classical central approach can be found in various papers (see for example [15,17,19,21,23]).

The construction of the central schemes is based on using the staggered grid. According to this, two sets of cells are introduced: the nonstaggered cells $I_i = [x_{i-\frac{1}{2}}, x_{i+\frac{1}{2}}]$, $i = 0, \ldots, N$ and the staggered cells $I_{i+\frac{1}{2}} = [x_i, x_{i+1}]$, $i = 0, \ldots, N-1$. We restrict our discussion on the uniform cell size Δx. The extension of the scheme to the nonuniform mesh is not possible here, since the conservative approximations to the flux function derivatives on the nonuniform mesh, obtained by the WENO reconstruction procedure, do not exist higher then second-order accurate [24]. The appropriate notations for the average value of the solution at time $t = t^n$ are used: $\overline{\mathbf{u}}_i^n$ denotes the average value of the solution over the nonstaggered cell I_i and $\overline{\mathbf{u}}_{i+\frac{1}{2}}^n$ denotes the average value over the staggered cell $I_{i+\frac{1}{2}}$. Integration of (1) over the control volume $I_{i+\frac{1}{2}} \times [t^n, t^{n+1}]$ gives

$$\overline{\mathbf{u}}_{i+\frac{1}{2}}^{n+1} = \overline{\mathbf{u}}_{i+\frac{1}{2}}^{n} - \frac{1}{\Delta x}\left[\int_{t^n}^{t^{n+1}} \mathbf{f}(\mathbf{u}(x_{i+1},t),x_{i+1})\,\mathrm{d}t - \int_{t^n}^{t^{n+1}} \mathbf{f}(\mathbf{u}(x_i,t),x_i)\,\mathrm{d}t\right] + \frac{1}{\Delta x}\int_{t^n}^{t^{n+1}}\int_{x_i}^{x_{i+1}} \mathbf{g}(\mathbf{u}(x,t),x)\,\mathrm{d}x\,\mathrm{d}t. \tag{13}$$

The expression (13) is used as the starting point of the central WENO scheme. All terms in this expression should be appropriately discretized. By following [20] first the staggered cell averages $\overline{\mathbf{u}}_{i+\frac{1}{2}}^n$ are evaluated by averaging the piecewise polynomial approximation

$$\widehat{\mathbf{P}}(x,\overline{\mathbf{u}}^n)=\sum_i \widehat{\mathbf{P}}_i(x)\chi_{I_i}(x), \tag{14}$$

whose average over each cell I_i coincide with the known cell averaged values $\overline{\mathbf{u}}_i^n$ (Fig. 2). $\widehat{\mathbf{P}}_i(x)$ are vectors of the polynomial approximations, which must be determined such that the staggered averaged values evaluated as

$$\overline{\mathbf{u}}_{i+\frac{1}{2}}^n=\frac{1}{\Delta x}\int_{I_{i+\frac{1}{2}}}\widehat{\mathbf{P}}(x,\overline{\mathbf{u}}^n)\,\mathrm{d}x=\frac{1}{\Delta x}\left[\int_{x_i}^{x_{i+\frac{1}{2}}}\widehat{\mathbf{P}}_i(x)\,\mathrm{d}x+\int_{x_{i+\frac{1}{2}}}^{x_{i+1}}\widehat{\mathbf{P}}_{i+1}(x)\,\mathrm{d}x\right] \tag{15}$$

become $(2r-1)$th-order accurate approximations to the averaged values of the solution. The required order of accuracy for integrals in (15) can be attained if they are found by the appropriate WENO reconstruction procedure. In the case of the constant cell sizes these integrals can be expressed as linear combinations with constant coefficients of the known values $\overline{\mathbf{u}}_i^n$, i.e., the relations

$$\frac{1}{\Delta x}\int_{x_{i-\frac{1}{2}}}^{x_i}\widehat{\mathbf{P}}_i(x)\,\mathrm{d}x=\sum_{s=0}^{r-1}\sum_{j=0}^{r-1}\widehat{\omega}_{r,s}(\overline{\mathbf{u}})b^-_{r,s,j}\overline{\mathbf{u}}_{i-r+1+s+j}, \tag{16}$$

$$\frac{1}{\Delta x}\int_{x_i}^{x_{i+\frac{1}{2}}}\widehat{\mathbf{P}}_i(x)\,\mathrm{d}x=\sum_{s=0}^{r-1}\sum_{j=0}^{r-1}\widehat{\omega}_{r,s}(\overline{\mathbf{u}})b^+_{r,s,j}\overline{\mathbf{u}}_{i-r+1+s+j} \tag{17}$$

are valid if $(r-1)$th degree polynomial reconstruction is used. Here, $b^-_{r,s,j}$ and $b^+_{r,s,j}$, $s,j=0,\ldots,r-1$ are the appropriate precomputed interpolation coefficients that do not depend on the reconstruction values. The nonlinear weights $\widehat{\omega}_{r,s}(\overline{\mathbf{u}}),s=0,\ldots,r-1$ are computed as usually in the WENO reconstruction procedure by using the linear weights, which are obtained by imposing the accuracy conditions for integrals in (16) and (17), and the smoothness indicators that are the smoothness measures of the reconstructed function $\mathbf{u}$. The detail description of the whole procedure can be found in [20,23]. The coefficients $b^-_{r,s,j}$ and $b^+_{r,s,j}$ for the cases $r=3$ and 5 are given in [23]. The linear weights that lead to $(2r-1)$th-order approximation in the

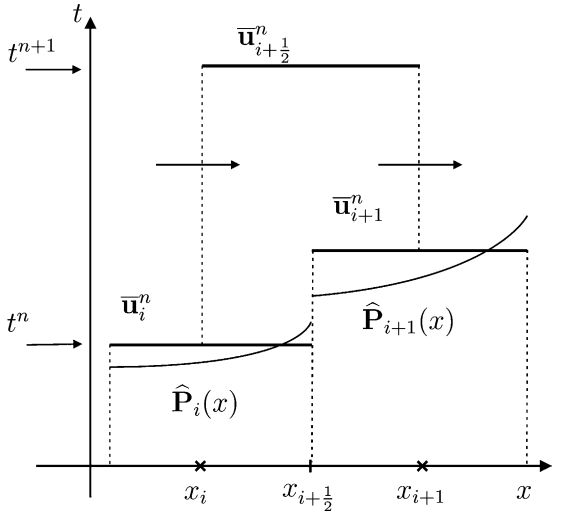

Fig. 2. Polynomial reconstructions and time evolution of the staggered average values in the central WENO scheme.

WENO reconstruction are also presented in [23]. In the expressions (16) and (17) for the WENO reconstructions, we use the componentwise approach, which means that all the operations and also the smoothness indicators evaluations have to be performed componentwise. However, there is a possibility of performing the WENO reconstructions on the local characteristic variable and then of transforming the obtained values back into physical space, as it is already mentioned in the previous section, but then the balanced numerical scheme cannot be obtained. A detailed study of both mentioned approaches is given in [23].

The second part of our central WENO scheme is related to the evaluation of the flux and the source term integrals in (13). Let us suppose that the CFL condition of the form

$$\Delta t < \frac{\Delta x}{2 \max_i \rho(\mathbf{A}(\overline{\mathbf{u}}_i))} \tag{18}$$

is satisfied, where ρ denotes the spectral radius of the Jacobian matrix $\mathbf{A}(\overline{\mathbf{u}}_i)$. Under that assumption the discontinuities starting from the boundaries of the cell I_i do not arrive to its center until the next time step, thus the values under the integrals in (13) remain smooth. Therefore, these integrals can be numerically approximated by using some classical approach. If we use the Gauss quadrature formula, we have

$$\int_{t^n}^{t^{n+1}} \mathbf{f}(\mathbf{u}(x_i,t),x_i)\,\mathrm{d}t \approx \Delta t \sum_{l=1}^{k} \alpha_l \mathbf{f}(\mathbf{u}(x_i,t^n+\beta_l\Delta t),x_i) \tag{19}$$

and

$$\int_{x_i}^{x_{i+1}} \int_{t^n}^{t^{n+1}} \mathbf{g}(\mathbf{u}(x,t),x)\,\mathrm{d}x\,\mathrm{d}t \approx \Delta t \Delta x \sum_{l=1}^{k} \alpha_l \widetilde{\mathbf{g}}(\mathbf{u}(x_i,t^n+\beta_l\Delta t),\mathbf{u}(x_{i+1},t^n+\beta_l\Delta t)). \tag{20}$$

The parameters α_l and β_l are the weights and the nodes of the particular quadrature formula. Similarly, the trapezoidal or Simpson formulas can be applied. In this work we typically use the three-point Gauss quadrature formula. There are two tasks in the expressions (19) and (20) that must be performed yet. First, the values $\mathbf{u}(x_i,t^n+\beta_l\Delta t)$ must be evaluated and second, the approximation $\widetilde{\mathbf{g}}(\mathbf{u}(x_i,t^n+\beta_l\Delta t),\mathbf{u}(x_{i+1},t^n+\beta_l\Delta t))$ to the source term has to be defined.

The approximations to the point values $\mathbf{u}(x_i,t^n+\beta_l\Delta t),\ l=1,\ldots,k$ can be found as the solutions of the Cauchy problem

$$\frac{\mathrm{d}\mathbf{u}(x_i,t)}{\mathrm{d}t} = -\mathbf{f}_x(\mathbf{u}(x,t),x)|_{x=x_i} + \mathbf{g}_i(t), \tag{21}$$

$$\mathbf{u}(x_i,t^n) \approx \mathbf{u}_i^n. \tag{22}$$

Here, the notation $\mathbf{g}_i(t)$ is used for the value of the source term at the considered time t at the point x_i, i.e., $\mathbf{g}_i(t)=\mathbf{g}(\mathbf{u}(x_i,t),x_i)$. The computation of (21) and (22) is divided into two separate tasks.

First, the initial condition $\mathbf{u}_i^n$ in (22) is computed from the known cell averages $\{\overline{\mathbf{u}}_i^n\}$ by the WENO reconstruction procedure. We take the WENO reconstruction that produces the approximation for the point value $\mathbf{u}(x_i,t^n)$ that is $(2r-1)$th-order accurate. When constant mesh size is used, the values obtained by this WENO reconstruction can be expressed as the linear combination of the values $\{\overline{\mathbf{u}}_i^n\}$, i.e.,

$$\mathbf{u}_i^n = \sum_{s=0}^{r-1} \sum_{j=0}^{r-1} \widetilde{\omega}_{r,s}(\overline{\mathbf{u}}^n) c_{r,s,j} \overline{\mathbf{u}}_{i-r+1+s+j}^n. \tag{23}$$

The constants $c_{r,s,j},\ s,j=0,\ldots,r-1$ are the appropriate interpolation coefficients. The weights $\widetilde{\omega}_{r,s}(\overline{\mathbf{u}}^n),\ s=0,\ldots,r-1$ are again computed by using the same smoothness indicators as before in (16) and (17), but with different linear weights obtained by imposing the required order of accuracy at the given point. For $r=3$ and 5, the coefficients $c_{r,s,j}$ and the linear weights can be found in [23].

If the values $\mathbf{u}(x_i,t^n+\beta_l\Delta t),\ l=1,\ldots,k$ are evaluated from the differential equation (21) by using the classical Runge–Kutta method, the complete evaluation procedure should be applied k times. Instead, we can reduce our computations if the natural continuous extension of the Runge–Kutta method is used (see [20,23] for details). In that case, at each time step, the Runge–Kutta method must be applied only once. According to the procedure that is described, for example, in [20,23], we proceed as follows. First, the classical v-stage Runge–Kutta method

$$\mathbf{u}_i^{n+1}=\mathbf{u}_i^n+\Delta t\sum_{j=1}^{v}b_j\mathbf{L}_i^{(j)} \tag{24}$$

is applied. Here, $\mathbf{L}_i^{(j)}$ denotes the approximation to the right-hand side of (21) at the state $\mathbf{u}_i^{(j)}=\mathbf{u}_i^n+\Delta t\sum_{k=1}^{j-1}a_{jk}\mathbf{L}_i^{(k)}$. The coefficients $b_j,\ j=1,\ldots,v$ and $a_{jk},\ j,k=1,\ldots,v$ are the known Runge–Kutta coefficients. By using the evaluated approximations $\mathbf{L}_i^{(j)}$ and appropriate polynomial coefficients $b_j(\theta)$ of the natural continuous extension of the Runge–Kutta scheme, the values $\mathbf{u}(x_i,t^n+\theta\Delta t),\ 0\leqslant\theta\leqslant 1$ can be approximated by using the formula

$$\mathbf{u}(x_i,t^n+\theta\Delta t)=\overline{\mathbf{u}}_i^n+\Delta t\sum_{j=1}^{v}b_j(\theta)\mathbf{L}_i^{(j)}. \tag{25}$$

The coefficients $b_j(\theta)$ can be found in [20,23]. Finally, by using (25), all the values $\mathbf{u}(x_i,t^n+\beta_l\Delta t),\ l=1,\ldots,k$ can be determined.

Now it remains to find the approximations of the right-hand side of (21), i.e., to find the values $\mathbf{L}_i^{(j)}$. Here, we follow the WENO reconstruction again. As the classical WENO schemes are based on imposing $(2r-1)$th-order accuracy on the cell boundaries, the approximation of the term $\partial_x\mathbf{f}(\mathbf{u}^{(j)},x)|_{x=x_i}$ can be evaluated by using the expression

$$\frac{1}{\Delta x}\left(\mathbf{f}^-_{i+\frac{1}{2}}-\mathbf{f}^+_{i-\frac{1}{2}}\right), \tag{26}$$

where $\mathbf{f}^-_{i+\frac{1}{2}}$ denotes the value of the polynomial approximation $\mathbf{P}_i(x)$ at the point $x_{i+\frac{1}{2}}$, while $\mathbf{f}^+_{i-\frac{1}{2}}$ represents its value at $x_{i-\frac{1}{2}}$. $\mathbf{P}_i(x)$ is here the $(2r-1)$th-order accurate polynomial approximation to the flux $\mathbf{f}$ obtained by the WENO reconstruction over all the stencils that include the point x_i. The values that are needed can be evaluated as the linear combinations

$$\mathbf{f}^-_{i+\frac{1}{2}}=\mathbf{P}_i(x_{i+\frac{1}{2}})=\sum_{s=0}^{r-1}\sum_{j=0}^{r-1}\omega_{r,s}(\mathbf{f})a^-_{r,s,j}\mathbf{f}_{i-r+1+s+j}, \tag{27}$$

$$\mathbf{f}^+_{i-\frac{1}{2}}=\mathbf{P}_i(x_{i-\frac{1}{2}})=\sum_{s=0}^{r-1}\sum_{j=0}^{r-1}\omega_{r,s+1}(\mathbf{f})a^+_{r,s+1,j}\mathbf{f}_{i-r+1+s+j}, \tag{28}$$

where $\mathbf{f}_i=\mathbf{f}(\mathbf{u}_i^{(j)},x_i)$. The coefficients $a^-_{r,s,j}$ and $a^+_{r,s,j},\ s,j=0,\ldots,r-1$ are the same as in (7) and the non-linear weights $\omega_{r,s}(\mathbf{f}),\ s=0,\ldots,r-1$ are also evaluated at the same manner as in (7). Finally, we can conclude that the presented approximation for the flux derivative is $(2r-2)$th-order accurate.

The source term at the point x_i that appears in (21) can be evaluated just pointwise, or some other approach depending on the particular conservation law can be used, as we will see in the proceeding of this work.

Let us resume the whole described procedure of the central WENO scheme. It could be divided in two steps, the predictor and the corrector step. In the predictor step the values $\mathbf{u}(x_i, t^n + \beta_l \Delta t),\ l = 1, \ldots, k$ should be determined from (21) and (22) by using (25). Here, the two WENO reconstructions are performed – the first one evaluates the approximations to the point values from the cell averages, while the second one approximates the flux derivative. In the corrector step of the scheme the obtained values are used in the expressions (19) and (20) that are included in (13) for evaluating the time evolution of the staggered average values (see Fig. 2). In this step the WENO reconstruction is used to evaluate the staggered average values. Such a defined numerical scheme is $(2r-1)$th-order accurate. Bearing in mind that the terms related to the source term evaluation, which are dependent on the particular balance law still need to be defined, we conclude the process of evaluation of the new staggered values $\overline{\mathbf{u}}_{i+\frac{1}{2}}^{n+1}$. With this, the time step in the classical central WENO scheme is finished. At the next time step, by applying the same procedure the new non-staggered values $\overline{\mathbf{u}}_i^{n+2}$ would be obtained.

However, we concentrate in this work on the nonstaggered central WENO scheme. That means at each time step we must return to the nonstaggered mesh. Following [15], after the staggered values $\overline{\mathbf{u}}_{i+\frac{1}{2}}^{n+1}$ are obtained, the nonstaggered values $\overline{\mathbf{u}}_i^{n+1}$ can be predicted by averaging the WENO reconstruction based on the obtained staggered values over the nonstaggered cells. Of course, a similar reconstruction as the one defined with (14)–(17) is used. We remark here that the nonstaggered approach is adequate for the balance laws that include some spatially dependent terms whose values are known at the centers x_i of the non-staggered cells I_i only, such is the case in this paper. The standard central WENO scheme would not be appropriate in that case.

4. Application to the open-channel flow and the shallow water equations

We study now the application of our schemes to the one-dimensional open-channel flow equations. They are obtained if in (1) we take

$$\mathbf{u} = \begin{pmatrix} A \\ Q \end{pmatrix}, \quad \mathbf{f} = \begin{pmatrix} Q \\ \frac{Q^2}{A} + gI_1 \end{pmatrix}, \quad \mathbf{g} = \begin{pmatrix} 0 \\ gI_2 - gA\frac{\mathrm{d}z}{\mathrm{d}x} - gAS_\mathrm{f} \end{pmatrix}. \tag{29}$$

Here, $A = A(x,t)$ is the wetted cross-section area, $Q = Q(x,t)$ is the discharge, g is the gravitational constant and $z = z(x)$ is the bed level. The additional terms in (29) are the hydrostatic pressure force term $I_1 = I_1(x,t)$ defined with

$$I_1(x,t) = \int_0^{h(x,t)} (h-\zeta) B(x,\zeta)\,\mathrm{d}\zeta, \tag{30}$$

the term $I_2 = I_2(x,t)$ that represents the forces related to changes of the channel width

$$I_2(x,t) = \int_0^{h(x,t)} (h-\zeta)\frac{\partial B}{\partial x}(x,\zeta)\,\mathrm{d}\zeta, \tag{31}$$

and the friction slope

$$S_\mathrm{f} = \frac{M^2 Q|Q|}{A^2 R^{4/3}}, \tag{32}$$

which models the friction forces through the channel. Here, $M = M(x)$ is the Manning's friction factor, while $R = R(x, A)$ is the cross-section hydraulic radius. The width of the cross-section area on the depth ζ, $B(x, \zeta)$, is connected with the wetted cross-section area by the following relation:

$$A(x,t) = \int_0^{h(x,t)} B(x,\zeta)\,\mathrm{d}\zeta, \tag{33}$$

where h is the water depth. $B(x, h)$ is the width of the free surface at the observed cross-section profile.

As a special case of the open-channel flow equations, where the width of the rectangular channel is constant, we obtain the shallow water equations, which are given with

$$\mathbf{u} = \begin{pmatrix} h \\ hv \end{pmatrix}, \quad \mathbf{f} = \begin{pmatrix} hv \\ hv^2 + \frac{1}{2}gh^2 \end{pmatrix}, \quad \mathbf{g} = \begin{pmatrix} 0 \\ gh(-\frac{\mathrm{d}z}{\mathrm{d}x} - \frac{M^2 v|v|}{h^{4/3}}) \end{pmatrix}. \tag{34}$$

Here, $v = v(x, t)$ denotes the water velocity. One can notice that by changing the variables (A, Q) with (h, hv), the expressions in (34) are obtained from (29). Thus, with the definitions of the terms that arise in the numerical schemes for the open-channel flow equations, the terms for the shallow water case will be automatically defined.

For the complete definition of the numerical schemes presented in the previous sections it remains to determine some terms. By imposing the requirement of preserving some steady-state solutions, we obtain the schemes that we refer to as to the balanced numerical schemes, since the zero time evolution in the case of the steady state implies that the flux gradient and the source term are in balance. It would be perfect if the balancing could be obtained on the numerical level too. Precisely, here we want that the numerical scheme preserves the quiescent flow exactly and we say that then it satisfies the exact conservation property. The solution in the case of the quiescent flow case is given with

$$h + z = H = \text{const.} \quad \text{and} \quad Q = 0. \tag{35}$$

Before we apply our numerical schemes, let us observe that in the case of the still water (35) the friction term disappears. Therefore, it will have no effect to the exact conservation property of the numerical schemes. In this paper the semi-implicit treatment of the friction term (see [4]) is used and it is excluded from the numerical source term definitions in the following sections.

4.1. Application of the finite volume WENO schemes

For the complete definition of the finite volume WENO scheme there are few terms that should be now defined. First, the term $\mathbf{V}(\mathbf{u}', \mathbf{u}'', x', x'')$ that appears in the relation (8) should numerically approximate the term

$$\mathbf{v}\,\mathrm{d}x = \begin{pmatrix} 0 \\ g\frac{\partial I_1}{\partial x}\big|_{A=\text{const.}} \end{pmatrix} \mathrm{d}x. \tag{36}$$

In [30], we showed that Eq. (8) is fulfilled if we define the Roe average $\widetilde{\mathbf{u}}_{\mathrm{Roe}}(\mathbf{u}', \mathbf{u}'')$ of the states $\mathbf{u}'$ and $\mathbf{u}''$ with

$$\widetilde{v}_{\mathrm{Roe}} = \frac{\sqrt{A'}v' + \sqrt{A''}v''}{\sqrt{A'} + \sqrt{A''}}, \tag{37}$$

where the relation $\widetilde{Q}_{\mathrm{Roe}} = \widetilde{A}_{\mathrm{Roe}}\widetilde{v}_{\mathrm{Roe}}$ is valid. The approximation for the average $\widetilde{A}_{\mathrm{Roe}}$ can be chosen arbitrarily and we use just

$$\widetilde{A}_{\mathrm{Roe}} = \frac{A' + A''}{2}. \tag{38}$$

By following [30], we approximate (36) with

$$\mathbf{V}(\mathbf{u}', \mathbf{u}'', x', x'') = \begin{pmatrix} 0 \\ g(I_1'' - I_1') - \widetilde{c}^2(A'' - A') \end{pmatrix}, \tag{39}$$

where $\widetilde{c}$ stands for the numerical approximation of the term $c = \sqrt{g(\partial I_1/\partial A)|_{x=\mathrm{const.}}}$. Since $(\partial I_1/\partial A)|_{x=\mathrm{const.}} = (A/B)$, the term c can be approximated as

$$\widetilde{c} = \sqrt{g\frac{\widetilde{A}_{\mathrm{Roe}}}{\widetilde{B}}}. \tag{40}$$

The approximation for $\widetilde{B}$ is still open and we use the simple arithmetic average.

If we suppose in the open-channel flow equations that $B = \text{const.}$, it follows that $A = hB$, $I_1 = \frac{1}{2}h^2B$ and $c = \sqrt{gh}$, thus the relation (39) becomes equal zero. This is what we expect, since in the shallow water case the flux is not spatially dependent.

At the $(i+\frac{1}{2})$th cell boundary the Roe average state is taken as $\widetilde{\mathbf{u}}_{i+\frac{1}{2}} = \widetilde{\mathbf{u}}_{\mathrm{Roe}}(\mathbf{u}^-_{i+\frac{1}{2}}, \mathbf{u}^+_{i+\frac{1}{2}})$. Similarly, the terms $\mathbf{V}_{i+\frac{1}{2}}$ and $c_{i+\frac{1}{2}}$ are predicted from (39) and (40) by including the values $\mathbf{u}^-_{i+\frac{1}{2}}$, $\mathbf{u}^+_{i+\frac{1}{2}}$, x_i and x_{i+1} instead of $\mathbf{u}'$, $\mathbf{u}''$, x' and x''. The eigenvalues $\lambda^{(p)}_{i+\frac{1}{2}}$, $p = 1, 2$, left and right eigenvectors, $\mathbf{l}^{(p)}_{i+\frac{1}{2}}$ and $\mathbf{r}^{(p)}_{i+\frac{1}{2}}$, $p = 1, 2$ of the Jacobian matrix at the state $\widetilde{\mathbf{u}}_{i+\frac{1}{2}}$ are evaluated from

$$\lambda^{(1)} = v - c, \quad \lambda^{(2)} = v + c, \tag{41}$$

$$\mathbf{l}^{(1)} = \frac{1}{2c}\begin{pmatrix} \lambda^{(2)} \\ -1 \end{pmatrix}, \quad \mathbf{l}^{(2)} = \frac{1}{2c}\begin{pmatrix} \lambda^{(1)} \\ 1 \end{pmatrix} \quad \text{and} \quad \mathbf{r}^{(p)} = \begin{pmatrix} 1 \\ \lambda^{(p)} \end{pmatrix}. \tag{42}$$

An important thing must be emphasized in connection with the evaluation of the states $\mathbf{u}^{\pm}_{i+\frac{1}{2}}$. The value of the first component A of the variable $\mathbf{u}$ at the cell boundary is not reconstructed directly. Instead, we proceed in the next way. We evaluate first the values h_i from the known values A_i. Then the values $h^{\pm}_{i+\frac{1}{2}}$ are determined by the WENO reconstruction, and finally, we use the obtained water depth at the cell interfaces to evaluate the corresponding wetted cross-section areas $A^{\pm}_{i+\frac{1}{2}}$.

Now the source term approximations should be defined. If we include the analytical connection $I_2 = (\partial I_1/\partial x) - A(\partial h/\partial x)$ into the source term (29), it is natural to take

$$\mathbf{G}_{i+\frac{1}{2}} = \mathbf{G}(\mathbf{u}^-_{i+\frac{1}{2}}, \mathbf{u}^+_{i+\frac{1}{2}}) = \begin{pmatrix} 0 \\ g(I^+_{1,i+\frac{1}{2}} - I^-_{1,i+\frac{1}{2}}) - gA_{i+\frac{1}{2}}(H^+_{i+\frac{1}{2}} - H^-_{i+\frac{1}{2}}) \end{pmatrix}, \tag{43}$$

where $H^{\pm}_{i+\frac{1}{2}} = h^{\pm}_{i+\frac{1}{2}} + z^{\pm}_{i+\frac{1}{2}}$. There are two possible ways to determine the values $H^{\pm}_{i+\frac{1}{2}}$. The first one is to use the values $H_i = h_i + z_i$ in the WENO reconstruction and to evaluate $H^{\pm}_{i+\frac{1}{2}}$ directly. The second one is to compute the heights of the riverbed $z^{\pm}_{i+\frac{1}{2}}$ at the $(i+\frac{1}{2})$th cell boundary and add it to $h^{\pm}_{i+\frac{1}{2}}$. We evaluate the terms $z^{\pm}_{i+\frac{1}{2}}$ from the known values z_i at the cell centers, by using the WENO reconstruction procedure with the smoothness indicators of the water depth variable h. Since the values $h^{\pm}_{i+\frac{1}{2}}$, which we need in that case have been already determined in the numerical flux evaluation, in both cases only one additional WENO reconstruction is needed.

The second part in the source term approximation that is essential for obtaining the balanced numerical scheme is given with

$$\mathbf{G}_{i,\mathrm{C}} = \mathbf{G}(\mathbf{u}^+_{i-\frac{1}{2}}, \mathbf{u}^-_{i+\frac{1}{2}}) = \begin{pmatrix} 0 \\ g(I^-_{1,i+\frac{1}{2}} - I^+_{1,i-\frac{1}{2}}) - g\frac{A^+_{i-\frac{1}{2}} + A^-_{i+\frac{1}{2}}}{2}(H^-_{i+\frac{1}{2}} - H^+_{i-\frac{1}{2}}) \end{pmatrix}. \tag{44}$$

In the shallow water case, the terms defined with (43) and (44) reduce to

$$\mathbf{G}_{i+\frac{1}{2}} = \mathbf{G}\left(\mathbf{u}^-_{i+\frac{1}{2}}, \mathbf{u}^+_{i+\frac{1}{2}}\right) = \begin{pmatrix} 0 \\ -g\frac{h^-_{i+\frac{1}{2}} + h^+_{i+\frac{1}{2}}}{2}\left(z^+_{i+\frac{1}{2}} - z^-_{i+\frac{1}{2}}\right) \end{pmatrix} \tag{45}$$

and

$$\mathbf{G}_{i,\mathrm{C}} = \mathbf{G}\left(\mathbf{u}^+_{i-\frac{1}{2}}, \mathbf{u}^-_{i+\frac{1}{2}}\right) = \begin{pmatrix} 0 \\ -g\frac{h^+_{i-\frac{1}{2}} + h^-_{i+\frac{1}{2}}}{2}\left(z^-_{i+\frac{1}{2}} - z^+_{i-\frac{1}{2}}\right) \end{pmatrix}, \tag{46}$$

respectively.

We claim that such a defined numerical scheme satisfies the exact conservation property. In order to establish this statement we must prove that under the quiescent flow condition (35) the numerical approximation of the space operator (5) is equal zero, i.e.,

$$\mathbf{L}_i = 0. \tag{47}$$

By including the definitions (6), (8), and (10)–(12) in (5), we obtain quite a large expression whose value should be zero. We divide this expression in few parts and prove that each of them is equal zero. The following relations have to be established

$$\mathbf{f}^+_{i+\frac{1}{2}} + \mathbf{f}^-_{i+\frac{1}{2}} - \mathbf{f}^+_{i-\frac{1}{2}} - \mathbf{f}^-_{i-\frac{1}{2}} - \left(\mathbf{G}_{i+\frac{1}{2}} + \mathbf{G}_{i-\frac{1}{2}} + 2\mathbf{G}_{i,\mathrm{C}}\right) = 0 \tag{48}$$

and

$$\mathbf{R}_{i+\frac{1}{2}}|\Lambda_{i+\frac{1}{2}}|\mathbf{L}_{i+\frac{1}{2}}\left(\mathbf{u}^+_{i+\frac{1}{2}} - \mathbf{u}^-_{i+\frac{1}{2}}\right) + \mathbf{R}_{i+\frac{1}{2}}\Lambda^{-1}_{i+\frac{1}{2}}|\Lambda_{i+\frac{1}{2}}|\mathbf{L}_{i+\frac{1}{2}}\mathbf{V}_{i+\frac{1}{2}} - \mathbf{R}_{i+\frac{1}{2}}\Lambda^{-1}_{i+\frac{1}{2}}|\Lambda_{i+\frac{1}{2}}|\mathbf{L}_{i+\frac{1}{2}}\mathbf{G}_{i+\frac{1}{2}} = 0. \tag{49}$$

Since in the quiescent flow case the first component of each term on the left-hand side of (48) is equal zero, it is enough to prove that the terms appearing in the second component of this expression vanish. With quite simple numerical calculations we can show that when the numerical fluxes in the quiescent flow case and expressions (43) and (44) are included in (48), the terms related to I_1 cancel out, therefore we only need to verify if the relations

$$H^\pm_{i+\frac{1}{2}} = h^\pm_{i+\frac{1}{2}} + z^\pm_{i+\frac{1}{2}} = H = \text{const.}, \quad i = 1, \ldots, N \tag{50}$$

hold. This is fulfilled for both the WENO reconstructions we propose before. Namely, since the equality

$$\sum_{s=s^\pm_{\min}}^{s^\pm_{\max}} \sum_{j=0}^{r-1} \omega_{r,s} a^\pm_{r,s,j} = 1, \tag{51}$$

is valid, in the first case, where the values $H^\pm_{i+\frac{1}{2}}$ are reconstructed from the values $H_i = h_i + z_i$, which are constant in the quiescent flow case, the relations (50) are obviously satisfied. In the second case, where the values $h^\pm_{i+\frac{1}{2}}$ and $z^\pm_{i+\frac{1}{2}}$ are reconstructed separately, but with the same weight values $\omega_{r,s} = \omega_{r,s}(h)$, we obtain

$$h^{\pm}_{i+\frac{1}{2}} + z^{\pm}_{i+\frac{1}{2}} = \sum_{s=s^{\pm}_{\min}}^{s^{\pm}_{\max}} \sum_{j=0}^{r-1} \omega_{r,s} a^{\pm}_{r,s,j} (h_{i-r+1+s+j} + z_{i-r+1+s+j}) = H. \tag{52}$$

The last equality follows from (51) and from the relations $h_i + z_i = H,\ i = 0, \ldots, N$. With this (48) is proved.

Now we concentrate on the left-hand side of (49). Under the quiescent flow assumptions, we obtain

$$\mathbf{R}_{i+\frac{1}{2}} |\Lambda_{i+\frac{1}{2}}| \mathbf{L}_{i+\frac{1}{2}} \left(\mathbf{u}^{+}_{i+\frac{1}{2}} - \mathbf{u}^{-}_{i+\frac{1}{2}} \right) = \begin{pmatrix} c_{i+\frac{1}{2}} (A^{+}_{i+\frac{1}{2}} - A^{-}_{i+\frac{1}{2}}) \\ 0 \end{pmatrix}, \tag{53}$$

and

$$\mathbf{R}_{i+\frac{1}{2}} \Lambda^{-1}_{i+\frac{1}{2}} |\Lambda_{i+\frac{1}{2}}| \mathbf{L}_{i+\frac{1}{2}} \mathbf{V}_{i+\frac{1}{2}} = \frac{1}{c_{i+\frac{1}{2}}} \begin{pmatrix} g(I^{+}_{1,i+\frac{1}{2}} - I^{-}_{1,i+\frac{1}{2}}) - c^{2}_{i+\frac{1}{2}} (A^{+}_{i+\frac{1}{2}} - A^{-}_{i+\frac{1}{2}}) \\ 0 \end{pmatrix}. \tag{54}$$

Moreover, for the part related to the source term approximation we find that

$$\mathbf{R}_{i+\frac{1}{2}} \Lambda^{-1}_{i+\frac{1}{2}} |\Lambda_{i+\frac{1}{2}}| \mathbf{L}_{i+\frac{1}{2}} \mathbf{G}_{i+\frac{1}{2}} = \frac{1}{c_{i+\frac{1}{2}}} \begin{pmatrix} g(I^{+}_{1,i+\frac{1}{2}} - I^{-}_{1,i+\frac{1}{2}}) - (A^{-}_{i+\frac{1}{2}} + A^{+}_{i+\frac{1}{2}})(H^{+}_{i+\frac{1}{2}} - H^{-}_{i+\frac{1}{2}}) \\ 0 \end{pmatrix}. \tag{55}$$

Finally, by putting together (53)–(55), and by using (50) we can easily see that (49) holds. With this the proof of the exact conservation property is finished. The same relations hold if the indices $(i + \frac{1}{2})$ are changed with $(i - \frac{1}{2})$. Finally, by putting together proved equations (48) and (49), we finish the proof of the exact conservation property for our scheme.

4.2. Application of the central WENO schemes

The first thing we must emphasize in connection with application of the nonstaggered central WENO schemes to the open-channel flow equations is that we could not obtain balancing for the channel with the arbitrary cross-sections, but only for the case of prismatic channel with variable width. In that case the channel cross-sections are rectangular and the relation $A = hB$ is valid.

For applying the central WENO schemes to the open-channel flow equations there are two terms corresponding to the source term approximation that still need to be determined. But there are also some additional corrections that we introduce when the central WENO schemes are applied to the considered balance law.

Let us consider the predictor step of the scheme. First, we adapt the flux derivative approximation at the point x_i that is defined with (26)–(28). However, we change this evaluation in order to obtain balancing between the flux gradient and the source term. More precisely, we change the terms $\mathbf{f}^{\pm}_{i+\frac{1}{2}}$ in (26) with terms $\widehat{\mathbf{f}}^{\pm}_{i+\frac{1}{2}}$, which are the WENO reconstruction values of the functions $\widehat{\mathbf{f}} = \mathbf{f} - \mathbf{f}_{I^{\pm}}$, where $I^{-} = i$ and $I^{+} = i + 1$. One can notice that the value of the derivative approximation will not change with this modification.

The term $\mathbf{g}_i(t)$ that arises in (21) we compute by using the decomposed approach

$$\mathbf{g}_i(t) = \mathbf{g}_{i,\mathrm{L}}(t) + \mathbf{g}_{i,\mathrm{R}}(t). \tag{56}$$

We define

$$\mathbf{g}_{i,\mathrm{R}}(t) = \frac{1}{\Delta x} \widehat{\mathbf{G}}^{-}_{i+\frac{1}{2}} \quad \text{and} \quad \mathbf{g}_{i,\mathrm{L}}(t) = \frac{1}{\Delta x} \widehat{\mathbf{G}}^{+}_{i-\frac{1}{2}}, \tag{57}$$

where $\widehat{\mathbf{G}}^{\pm}_{i+\frac{1}{2}}$ denote the values of the WENO reconstruction procedure (27) on the $(i+\frac{1}{2})$th cell boundary for the functions

$$\widehat{\mathbf{G}}^{\pm} = \begin{pmatrix} 0 \\ \pm g(I_1 - I_{1,I^{\pm}}) \mp g\frac{A+A_{I^{\pm}}}{2}(H - H_{I^{\pm}}) \end{pmatrix}, \tag{58}$$

with $I^- = i$ and $I^+ = i+1$. Thus, the approximation $\mathbf{L}_i^{(j)}$ to the right-hand side of (21) can be written in the form

$$\mathbf{L}_i^{(j)} = -\frac{1}{\Delta x}\left(\widehat{\mathbf{f}}^-_{i+\frac{1}{2}} - \widehat{\mathbf{f}}^+_{i-\frac{1}{2}} - \widehat{\mathbf{G}}^-_{i+\frac{1}{2}} - \widehat{\mathbf{G}}^+_{i-\frac{1}{2}}\right). \tag{59}$$

Moreover, instead of using the smoothness indicators for each of the functions $\widehat{\mathbf{f}}^{\pm}$ and $\widehat{\mathbf{G}}^{\pm}$ separately, we use the smoothness indicators of the functions $\widehat{\mathbf{f}}^{\pm} \pm \widehat{\mathbf{G}}^{\pm}$. More precisely, when the terms $\widehat{\mathbf{f}}^-_{i+\frac{1}{2}}$ and $\widehat{\mathbf{G}}^-_{i+\frac{1}{2}}$ are evaluated we use the smoothness measures of the function $\widehat{\mathbf{f}}^- - \widehat{\mathbf{G}}^-$, and for $\widehat{\mathbf{f}}^+_{i-\frac{1}{2}}$ and $\widehat{\mathbf{G}}^+_{i-\frac{1}{2}}$ the smoothness measures that belong to the function $\widehat{\mathbf{f}}^+ + \widehat{\mathbf{G}}^+$.

In the corrector step we define first the approximation for the source term that appears in (20) with

$$\widetilde{\mathbf{g}}(\mathbf{u}(x_i,t),\mathbf{u}(x_{i+1},t)) = \frac{1}{\Delta x}\begin{pmatrix} 0 \\ g(I_1(x_{i+1},t) - I_1(x_i,t)) - g\frac{A(x_i,t)+A(x_{i+1},t)}{2}(H(x_{i+1},t) - H(x_i,t)) \end{pmatrix}. \tag{60}$$

In the shallow water case the same algorithm is used and the terms defined with (58) and (60) reduce in the similar way as the source terms that appear in the finite volume WENO schemes.

What we have to do now is to concentrate on the algorithm of passing from the nonstaggered values $\overline{\mathbf{u}}_i^n$ to the staggered ones, $\overline{\mathbf{u}}^n_{i+\frac{1}{2}}$, and also, after the time evolution of the staggered values is applied and the values $\overline{\mathbf{u}}^{n+1}_{i+\frac{1}{2}}$ are computed, on the algorithm of returning to the nonstaggered mesh with the new obtained values $\overline{\mathbf{u}}_i^{n+1}$. In order to obtain balanced numerical scheme the algorithm is adapted, but only in the first component of $\mathbf{u}$. Since we consider here only rectangular channels, the relation $A = hB$ holds. First, instead of evaluating the values $A^n_{i+\frac{1}{2}}$, as the average value of the WENO reconstruction over the cell $I_{i+\frac{1}{2}}$, we apply the WENO reconstruction to the function $H = \frac{A}{B} + z$ and then by using (15)–(17), we obtain the values $H^n_{i+\frac{1}{2}}$. Moreover, the connection between the time evolution of $H^n_{i+\frac{1}{2}}$ and the time evolution of $A^n_{i+\frac{1}{2}}$ is given through the relation $\Delta H/\Delta t = (1/B)(\Delta A/\Delta t)$, since the riverbed z does not vary with time. After the values $H^{n+1}_{i+\frac{1}{2}}$ are determined, in the process of obtaining the nonstaggered values back, we again use the water level variable H and evaluate H_i^{n+1}. Finally, by applying the simple relation $A_i^{n+1} = B_i(H_i^{n+1} - z_i)$ the new nonstaggered values $\overline{\mathbf{u}}_i^{n+1}$ are evaluated.

At this point it is clear that the described procedure could not be applied to the arbitrary cross-section channel. Namely, in general case there exists no relation for obtaining the time evolution of $H^n_{i+\frac{1}{2}}$ from the time evolution of $A^n_{i+\frac{1}{2}}$ since these values are connected with the integral (33) and moreover, both are averaged over the staggered cell.

We want to prove now that the defined numerical scheme preserves the quiescent flow. The proof is divided in three steps. In the first one we prove that the time evolution in the predictor step of the scheme is equal zero. That is the case if the relations

$$\mathbf{L}_i^{(j)} = 0, \quad j = 1,\ldots,v \tag{61}$$

are valid. In the second step we want to prove that the time evolution in the corrector step is also equal zero. Finally, in the last step we must prove that the transformations from the nonstaggered to the staggered mesh and in the opposite direction preserves the quiescent flow values.

Since for both terms that appear in $\widehat{\mathbf{f}}^-_{i+\frac{1}{2}} - \widehat{\mathbf{G}}^-_{i+\frac{1}{2}}$, we use the same linear weights in the WENO reconstruction, the given difference is actually the WENO reconstruction of the function $\widehat{\mathbf{f}}^- - \widehat{\mathbf{G}}^-$. In the same

way $\widehat{\mathbf{f}}^+_{i-\frac{1}{2}} + \widehat{\mathbf{G}}^+_{i-\frac{1}{2}}$ is the WENO reconstruction for $\widehat{\mathbf{f}}^+ + \widehat{\mathbf{G}}^+$. According to the WENO reconstruction process the equalities

$$\widehat{\mathbf{f}}^-_k - \widehat{\mathbf{G}}^-_k = 0 \quad \text{and} \quad \widehat{\mathbf{f}}^+_k + \widehat{\mathbf{G}}^+_k = 0, \qquad k = 0, \ldots, N, \tag{62}$$

would imply $\widehat{\mathbf{f}}^-_{i-\frac{1}{2}} - \widehat{\mathbf{G}}^-_{i-\frac{1}{2}} = 0$ and $\widehat{\mathbf{f}}^+_{i-\frac{1}{2}} + \widehat{\mathbf{G}}^+_{i-\frac{1}{2}} = 0$, and therefore imply the validity of (61) also. The relations (62) are very easy to check, so we omit the proof here. With this we have proved that the numerical approximation of the right-hand side of (21) is equal zero, and therefore we have

$$\mathbf{u}_i^{n+1} = \mathbf{u}_i^n \quad \text{and} \quad \mathbf{u}_i^{(j)} = \mathbf{u}_i^n, \qquad j = 1, \ldots, v. \tag{63}$$

As the consequence of that, we obtain

$$\mathbf{u}(x_i, t^n + \beta_l \Delta t) = \mathbf{u}_i^n, \quad l = 1, \ldots, k. \tag{64}$$

By including the expressions (19), (20), and (60) in (13), and by using (64), we find that in the quiescent flow case the staggered values do not evolve in time. That means

$$\overline{\mathbf{u}}^{n+1}_{i+\frac{1}{2}} = \overline{\mathbf{u}}^n_{i+\frac{1}{2}}. \tag{65}$$

The last step of the proof is to check whether the finally obtained nonstaggered values, under the quiescent flow conditions, satisfy

$$\overline{\mathbf{u}}_i^{n+1} = \overline{\mathbf{u}}_i^n. \tag{66}$$

With that the exact conservation property of the proposed numerical scheme will be established.

Notice first that the second component of the variable $\mathbf{u}$ is equal zero in the quiescent flow case. This is the case for the nonstaggered values and for the staggered once too. Hence, we concentrate just on the first component of the variable $\mathbf{u}$. Because of $(A_i^n/B) + z_i = H_i = \text{const.}, \ i = 1, \ldots, N$ the WENO reconstruction of H will be constant, so the average values $H^n_{i+\frac{1}{2}}$ of that WENO reconstruction will have the same values for $i = 1, \ldots, N$. As the consequence of (65), that constant value of H remains the same at the new time level. The process of obtaining the nonstaggered values H_i^{n+1} is done again by WENO reconstruction and will obviously give us the same value. At the end the values A_i^{n+1} will also remain the same. With that the exact conservation property is proved.

5. Numerical results

We apply the presented schemes to both balance laws considered in this paper. With the numerical results we want to show the improvement achieved with the modified version of the schemes in comparison with the standard ones. We also compare our schemes with some other numerical schemes that are developed for the shallow water and the open-channel flow equations, such as the balanced first-order Roe [2] and the balanced second-order flux limited scheme [9] with the minmod limiter function [19].

In all the tests where the finite volume WENO schemes are applied, they are used with the third-order Runge–Kutta time integration. In the WENO reconstructions only the componentwise approach is used. Furthermore, the central WENO schemes with $r = 3$ are combined with the second-order Runge–Kutta method, while for the case $r = 5$, the fourth-order Runge–Kutta method is used. Both Runge–Kutta methods are used with their appropriate natural continuous extensions of the same order. If not stated otherwise, the channels in the test cases are supposed to be frictionless.

5.1. Shallow-water equations

5.1.1. An accuracy test over an exponential bump

First, we perform an accuracy test for the developed numerical schemes. In this problem the riverbed is defined with

$$z(x) = 0.2 \exp\left[-\frac{4}{25}(x-10)^2\right] \tag{67}$$

over the domain [0,20]. On the left boundary constant discharge equal 1 m^2/s is imposed, while on the right boundary the water depth of 1 m is fixed. The initial water level is defined as the stationary solution related to the constant discharge of 1 m^2/s. It can be evaluated analytically and is presented in Fig. 3. Since the numerical scheme is actually designed such that only the quiescent flow is exactly preserved, here, for the stationary solution, some numerical errors depending on the used space step occur. As we already stated the third order Runge–Kutta method is used when the finite volume WENO schemes are considered. In order to compensate for the lower order of temporal accuracy, we adjust the time step to $\Delta t \propto (\Delta x)^{R/3}$, so that the third-order Runge–Kutta time integration is effectively Rth order, where $R = 2r - 1$ stands for the accuracy of the WENO reconstruction. In such a way the time and the spatial accuracy become of the same order and we can check for the order of accuracy of our schemes. We compute the solution up to $t = 0.0001$ s. In Tables 1 and 2, we present the accuracy test results and computed orders of accuracy of the considered WENO schemes. In order to make a comparison, we present the orders of accuracy for the pointwise finite volume WENO schemes also (Table 1). Let us remember that the original WENO schemes are $R = 2r - 1$-order accurate. We can see that the numerical errors and orders of accuracy are similar for the pointwise and the balanced versions of schemes. Therefore, we can conclude that the orders of accuracy are not deteriorated with the reformulations introduced in this work for the considered balance law. All the schemes actually achieve their designed order of accuracy except for the higher-order finite volume WENO schemes. The reason of this reduced order of accuracy does not lie in the reformulation of the scheme but it is the consequence of the accumulation of the round-off errors when large number of numerical operations are executed. For the central WENO scheme one can note that the orders of accuracy correspond to the theoretical ones, but the L_1 and L_∞ errors are greater then in the finite volume WENO case. We think that the main reason of such a behaviour lies in averaging of the variables in each step of the scheme.

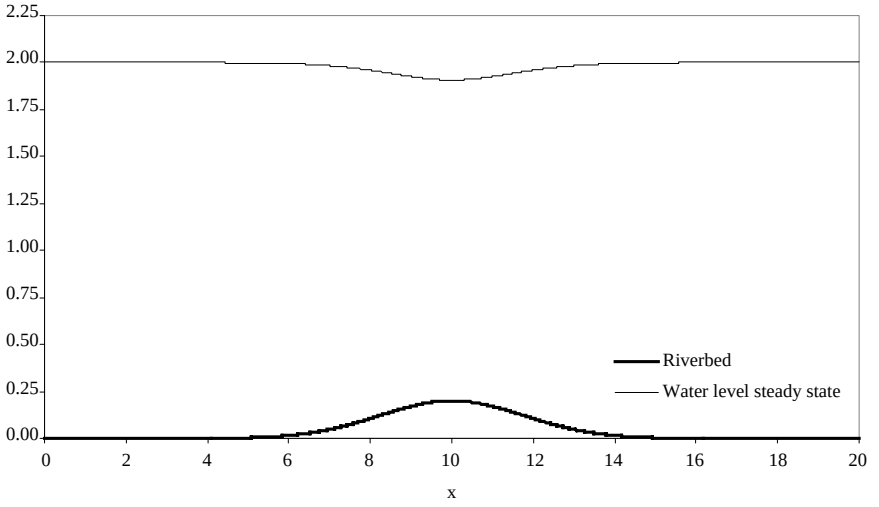

Fig. 3. Initial conditions for the test problem 5.1.1.

Table 1
Accuracy of the balanced finite volume WENO (test problem 5.1.1)

r	N	Balanced				Pointwise			
		L_1 error	L_1 order	L_∞ error	L_∞ order	L_1 error	L_1 order	L_∞ error	L_∞ order
2	40	3.95×10^{-8}		1.13×10^{-8}		5.92×10^{-7}		2.13×10^{-7}	
	80	7.39×10^{-9}	2.42	2.72×10^{-9}	2.05	1.60×10^{-7}	1.88	1.09×10^{-7}	0.97
	160	1.05×10^{-9}	2.81	4.18×10^{-10}	2.70	3.98×10^{-8}	2.01	5.47×10^{-8}	0.99
	320	2.86×10^{-10}	1.88	1.60×10^{-10}	1.39	9.60×10^{-9}	2.05	2.46×10^{-8}	1.15
3	40	1.05×10^{-8}		3.10×10^{-9}		3.10×10^{-8}		8.08×10^{-9}	
	80	5.32×10^{-10}	4.30	2.01×10^{-10}	3.95	1.37×10^{-9}	4.49	5.56×10^{-10}	3.86
	160	2.02×10^{-11}	4.72	1.11×10^{-11}	4.17	4.76×10^{-11}	4.85	2.33×10^{-11}	4.58
	320	7.79×10^{-13}	4.70	5.50×10^{-13}	4.34	1.63×10^{-12}	4.87	7.80×10^{-13}	4.90
4	20	4.12×10^{-8}		1.22×10^{-8}		1.50×10^{-7}		4.57×10^{-8}	
	40	2.19×10^{-9}	3.10	1.78×10^{-9}	2.77	4.52×10^{-9}	5.05	3.47×10^{-9}	3.72
	80	4.70×10^{-11}	5.54	5.24×10^{-11}	5.09	7.98×10^{-11}	5.82	8.91×10^{-11}	5.28
	160	6.26×10^{-13}	6.23	1.06×10^{-12}	5.63	1.09×10^{-12}	6.20	1.99×10^{-12}	5.48
5	20	4.56×10^{-8}		1.70×10^{-8}		8.65×10^{-8}		3.33×10^{-8}	
	40	6.92×10^{-10}	6.04	4.12×10^{-10}	5.36	7.20×10^{-10}	6.91	4.03×10^{-10}	6.37
	80	3.20×10^{-12}	7.75	1.91×10^{-12}	7.75	3.14×10^{-12}	7.84	1.82×10^{-12}	7.79
	160	4.00×10^{-14}	6.32	1.02×10^{-14}	7.55	1.49×10^{-13}	4.40	3.20×10^{-13}	2.51
6	20	3.00×10^{-8}		1.07×10^{-8}		4.67×10^{-8}		1.82×10^{-8}	
	40	4.12×10^{-10}	6.19	2.46×10^{-10}	5.44	4.31×10^{-10}	6.76	2.72×10^{-10}	6.06
	80	2.53×10^{-12}	7.34	1.28×10^{-12}	7.59	4.43×10^{-13}	9.93	2.50×10^{-13}	10.09
	160	3.75×10^{-14}	6.08	1.02×10^{-14}	6.97	5.38×10^{-14}	3.04	2.00×10^{-14}	3.65

Table 2
Accuracy of the balanced central WENO schemes (test problem 5.1.1)

r	N	L_1 error	L_1 order	L_∞ error	L_∞ order
3	20	2.43×10^{-2}		7.16×10^{-3}	
	40	1.40×10^{-3}	4.11	4.19×10^{-4}	4.09
	80	3.91×10^{-5}	5.16	1.74×10^{-5}	4.59
	160	7.09×10^{-7}	5.79	4.50×10^{-7}	5.27
	320	1.15×10^{-8}	5.95	7.92×10^{-9}	5.82
5	20	8.34×10^{-3}		3.20×10^{-3}	
	40	1.03×10^{-4}	6.34	5.20×10^{-5}	5.94
	80	2.06×10^{-7}	8.96	1.18×10^{-7}	8.78
	160	4.78×10^{-10}	8.76	3.49×10^{-10}	8.40

It would be interesting to compare the presented numerical errors and orders of accuracy for the WENO schemes with errors and orders of some first and second-order schemes. Therefore, we evaluate the numerical errors and orders of accuracy for the balanced first-order Roe and the second-order flux limited scheme (Table 3). One can notice that for the considered steady-state test problem the achieved orders of accuracy are higher then theoretical ones.

5.1.2. LeVeque test example over bump

In this test problem suggested by LeVeque [18], we want to compute the solutions obtained when a small perturbation of the initially still water arises. In this way we test whether the numerical scheme attains the correct wave speed propagation. The bottom topography is defined with

Table 3
Accuracy of the balanced first-order Roe and the balanced second-order flux limited scheme (test problem 5.1.1)

Numerical method	N	L_1 error	L_1 order	L_∞ error	L_∞ order
First-order Roe	20	4.17×10^{-9}		8.97×10^{-10}	
	40	5.33×10^{-10}	2.97	1.44×10^{-10}	2.64
	80	7.05×10^{-11}	2.92	2.03×10^{-11}	2.82
	160	8.93×10^{-12}	2.98	2.62×10^{-12}	2.95
Second-order flux limited	20	1.41×10^{-9}		2.80×10^{-10}	
	40	7.02×10^{-11}	4.33	3.25×10^{-11}	3.13
	80	5.06×10^{-12}	3.79	1.84×10^{-12}	4.12
	160	3.62×10^{-13}	3.80	1.10×10^{-13}	4.06

$$z(x) = \begin{cases} 0.25(\cos(10\pi(x-0.5))+1) & \text{if } |x-0.5| < 0.1, \\ 0 & \text{otherwise} \end{cases} \tag{68}$$

over a domain $[0,1]$. The initial conditions are

$$h(x,0) = \begin{cases} 1.0 - z(x) + \epsilon & \text{if } 0.1 < x < 0.2, \\ 1.0 - z(x) & \text{otherwise} \end{cases} \quad \text{and} \quad v(x,0) = 0. \tag{69}$$

As in [18] we take $g = 1$. The initial perturbation splits into two waves that propagate in opposite directions. All the numerical results are presented at time $t = 0.7$ s when the left moving wave already leaves the numerical domain, while the right going wave passes over the bump. In this test example we consider our schemes from different viewpoints.

First, we take $\epsilon = 0.001$. Since the main contribution of the schemes proposed in the paper is balancing, it is natural to show the comparison of the balanced and the pointwise versions of proposed schemes. In Fig. 4, we present results obtained with the finite volume WENO schemes for $r = 4$ at $t = 0.7$ s. In both versions we take $c_{\mathrm{CFL}} = 0.7$ and the space step $\Delta x = 0.005$. The oscillations that arise when the source term is pointwise evaluated can be clearly observed in both figures. Since the magnitude of the oscillations is of the same order as the initial perturbation, the pointwise scheme becomes unusable in such problems. It is true that for a bigger initial perturbation the oscillations that appear when the pointwise scheme is used cannot be seen on the global scale.

Now we want to compare the computational costs of the proposed schemes against some other well-known numerical schemes of the first and the second order. Since the main advantage of the WENO schemes are their high resolution properties, it is natural to compare the CPU times that are needed to achieve the solutions that overlay well. The similar type CPU time analysis is done in [32]. The test is performed on the problem with $\epsilon = 0.2$. The numerical solutions at time $t = 0.7$ s computed by using different schemes with $c_{\mathrm{CFL}} = 0.9$ are observed.

First, we compare the computational costs of the balanced finite volume WENO scheme and the balanced first-order Roe scheme. The main advantage of the Roe scheme is that it is computationally fast. But, since the scheme is quite diffusive, to achieve approximately the same resolution as with the WENO scheme, the grid must be refined. Particularly, from Fig. 5, where the solutions computed with the finite volume WENO scheme with $r = 3$ on 400 cells, and with the first-order Roe scheme on 800 and 1600 cells are presented, we can conclude that for achieving the same accuracy with the first-order Roe scheme, approximately four times finer mesh must be used. In Table 4, we present the CPU times that belong to the solutions presented in Fig. 5. Although the computational cost per one grid cell of the WENO scheme is much higher then for the first-order Roe scheme, it is still more efficient.

The comparison is also made between the balanced versions of the second order flux limited scheme with the minmod limiter function, the finite volume WENO scheme with $r = 4$, and the central WENO scheme

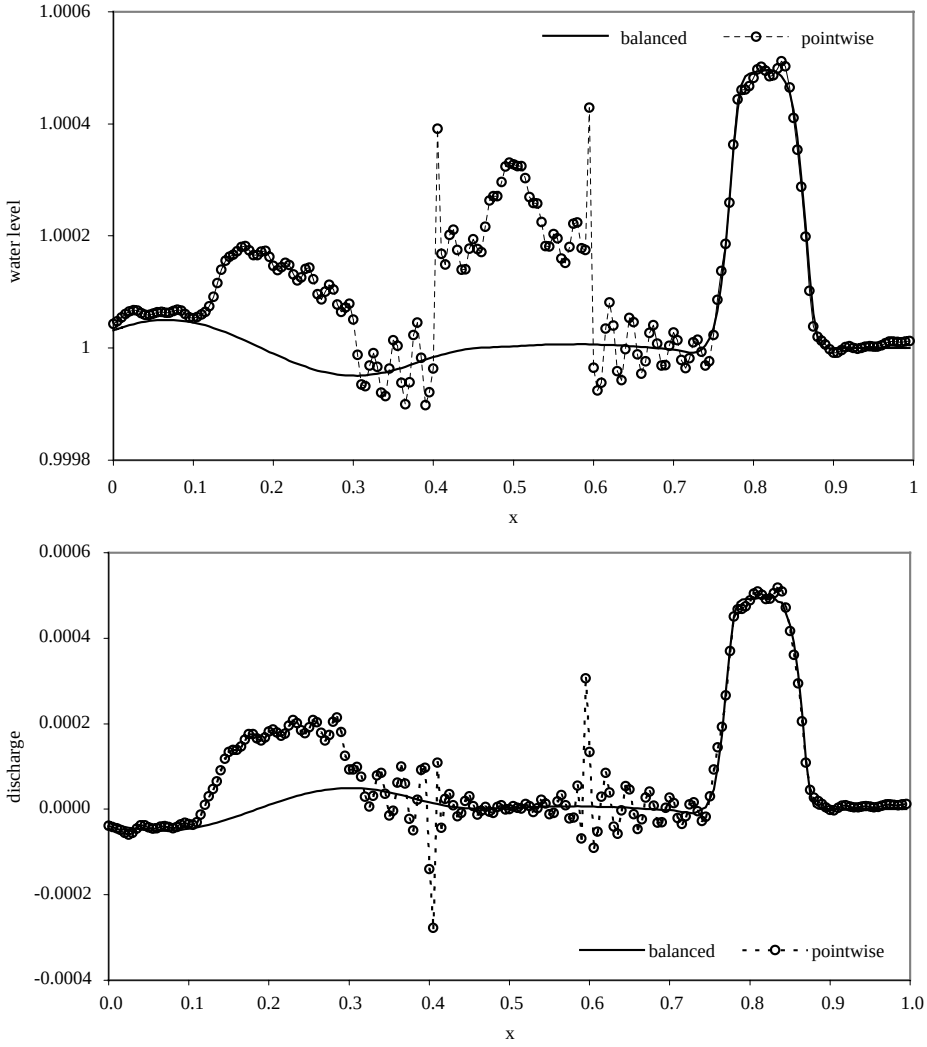

Fig. 4. Comparison of numerical results obtained with the finite volume WENO scheme, $r = 4$ (test problem 5.1.2). Top: water level at 0.7 s; Bottom: discharge at 0.7 s.

with $r = 3$. It is well known that the considered second-order scheme is very simple, fast and less diffusive then the first-order Roe scheme. Hence, to achieve the same accuracy as with the finite volume WENO scheme with $r = 4$ on 400 cells, just the two times finer grid (800 cells) must be used. The results are presented in Fig. 5. There also the numerical solution obtained with the central WENO scheme with $r = 3$, 400 cells, and by using $c_{\mathrm{CFL}} = 0.5$ is shown. The presented solutions coincide quite well. The CPU times needed for this computations are also presented in Table 4. From the obtained results it seems that for practical use the second-order flux limited scheme is actually better then the presented higher-order finite volume WENO scheme.

We can also compare the presented schemes with some other, more recently proposed schemes for the shallow water equations. In particular in [5], the authors proposed a wide class of first and second-order numerical schemes for the shallow water equations with source terms (among others the first-order Roe and

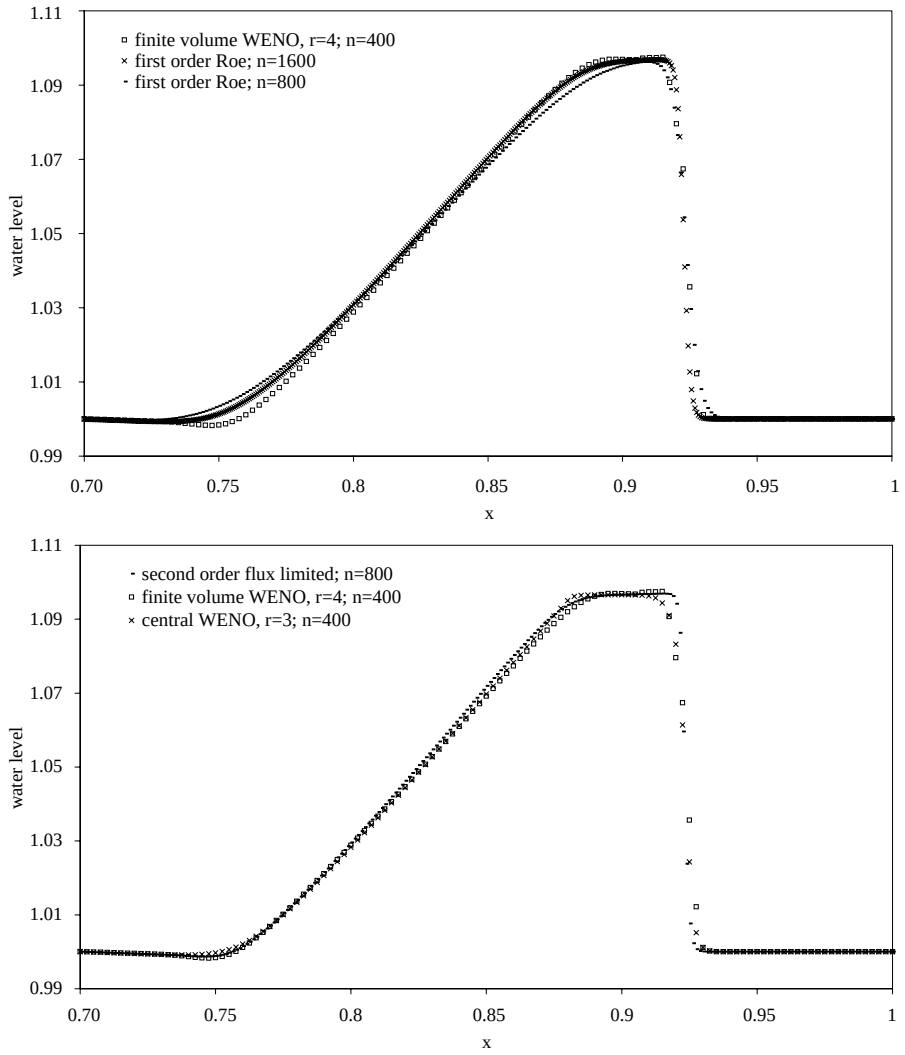

Fig. 5. Water level at $t = 0.7$ s in the test problem 5.1.2. Top: Comparison between first-order Roe scheme with 800 and 1600 points, and finite volume WENO scheme, $r = 3$ with 400 points; Bottom: Comparison between second-order flux limited scheme with 800 points, finite volume WENO scheme, $r = 4$ with 400 points, and central WENO scheme, $r = 3$ with 400 points.

Table 4
CPU times for different numerical schemes (test problem 5.1.2)

Numerical method	r	Number of cells	CPU time (s)
Finite volume WENO	3	400	4.45
First-order Roe		800	3.93
First-order Roe		1600	13.26
Finite volume WENO	4	400	5.86
Central WENO	3	400	3.66
Second-order flux limited		800	4.40

the second-order flux-limited scheme were also included there). Some of the proposed flux-splitted schemes were compared in [6] with the first-order Roe scheme. Since the authors of that paper conclude that their computational costs are very similar and that the schemes provide very close solutions, except in the critical points where the Roe scheme needs some entropy corrections, we consider the investigations we made here are sufficient to demonstrate the computational efficiency of the schemes proposed in this paper.

5.1.3. Test problems for transcritical flows over bump

This is a classical test problem for the steady-state flow [2]. The bump in the riverbed is defined with

$$z(x) = \begin{cases} 0.2 - 0.05(x-10)^2 & \text{if } 8 < x < 12, \\ 0 & \text{otherwise} \end{cases} \tag{70}$$

in the computational domain 25 m long. Depending on the boundary conditions we set, the flow can be subcritical all over the domain, it can become and stay supercritical, or become supercritical and then return to the subcritical. We consider here just the last case in which the hydraulic jump occurs. To obtain a hydraulic jump the discharge on the upstream boundary is set to 0.18 m^2/s, while on the downstream boundary constant water elevation $h(25,t) = 0.33$ m is imposed. In the computations a space step $\Delta x = 0.25$ m and $c_{\mathrm{CFL}} = 0.75$ are used. Although the improvements obtained by using the balanced treatment of the source term versus the pointwise source term evaluation are not so emphasized, they are still visible. But instead of the comparison between the balanced and the pointwise version of the scheme we found more important to compare finite volume WENO scheme with the second order flux limited scheme, and with the analytical solution. In Fig. 6, we can observe the good agreement of both schemes with analytical water level solution. The improvement of the finite volume WENO schemes against flux limited scheme can be nicely seen in the discharge, where the consistency error that arise in the critical point is much smaller when the finite volume WENO scheme is used then in the case when the flux limited scheme is. The comparison with the Roe scheme and also with some other first-order schemes is omitted here, since the conclusions and the results would be very similar.

5.1.4. Dam-break over a rectangular bump

Now, we verify our schemes on the dam-break problem over the discontinuous riverbed. The test case is taken from [29].

The riverbed is defined as

$$z(x) = \begin{cases} 8 & \text{if } |x - 1500/2| < 1500/8, \\ 0 & \text{otherwise,} \end{cases} \tag{71}$$

while the initial conditions are

$$H(x,0) = \begin{cases} 20 & \text{if } x \leqslant 750, \\ 15 & \text{otherwise} \end{cases} \quad \text{and } v(x,0) = 0 \tag{72}$$

(see Fig. 7). In this test problem the friction forces are also taken into account and the Manning friction factor is set to 0.1 over the whole numerical domain. The computations are performed with the space step $\Delta x = 5$ m and by using $c_{\mathrm{CFL}} = 0.5$. In Fig. 8, we present results obtained with the pointwise and the balanced version of the central WENO schemes, $r = 5$ at $t = 15$ s. The improvements obtained by using the balanced version are clearly visible. If we observe the numerical errors that appear when the nonbalanced central WENO scheme is used, we can notice that they are spread almost symmetrically around the two positions of the jumps in the riverbed. Actually, the initial numerical errors appear just over the jump and then this artificial disturbances propagates in both directions. As consequence the obtained numerical results are inaccurate.

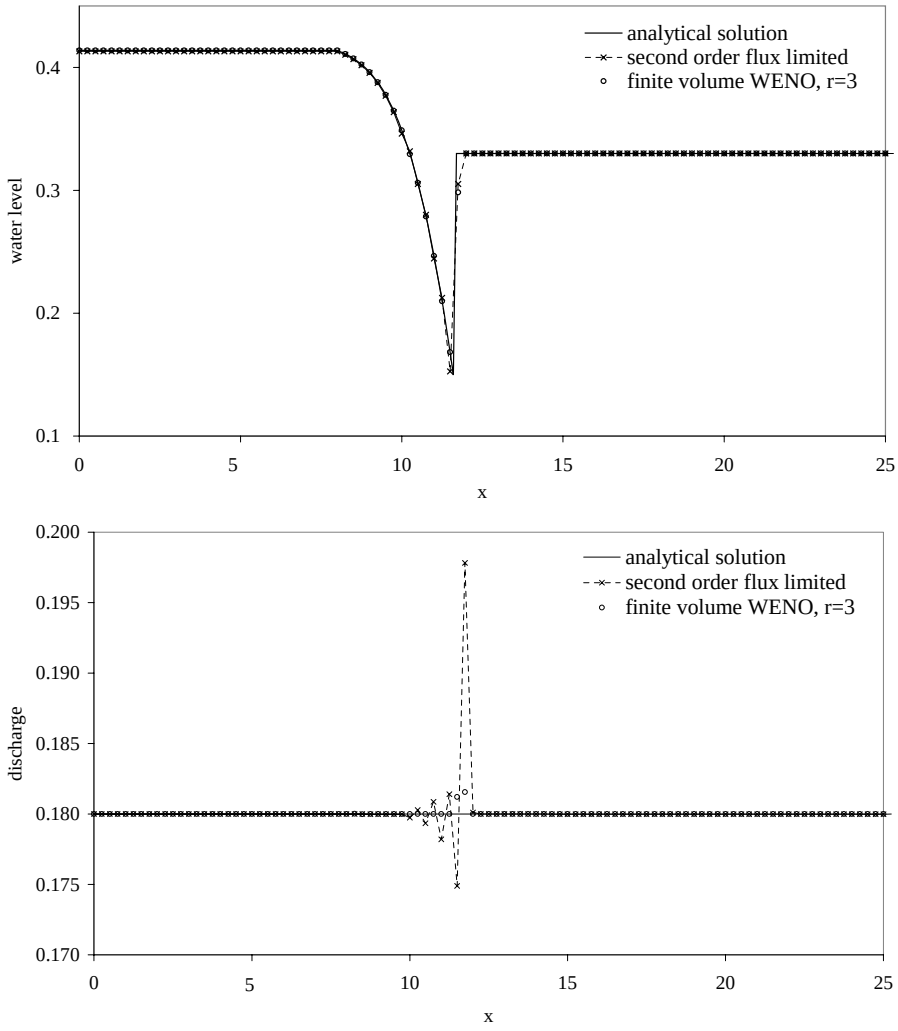

Fig. 6. Comparison of the numerical schemes and analytical solution. Steady hydraulic jump over bump (test problem 5.1.3). Top: water level; Bottom: discharge.

5.1.5. Dam-break experiment

In this test problem we compare the numerical results obtained by using the balanced finite volume WENO schemes with the experimental data. The measurements of this dam-break flow were performed in the Universitè libre de Bruxelles (ULB)/LRH-Châtelet by J.M. Hiver. The length of the channel is 38 m, the gate of the dam are placed at 15.5 m from the left, while 10 m to the right from the gate a triangular obstacle 0.4 m height and 6 m length appears (Fig. 9). Lengths of the slope on each side of the obstacle are 3 m. We consider here two test cases. In both cases the water is initially at rest and the water level in the reservoir is 0.75 m. In the first test case the channel on the right side of the gate is completely dry. On the outflow boundary a free outflow condition is supposed. In the second test downstream of the gate the channel is dry, except for a pool of steel water 0.15 m high that is bounded by the obstacle and a vertical wall on the downstream boundary. The described initial conditions are presented in Fig. 9.

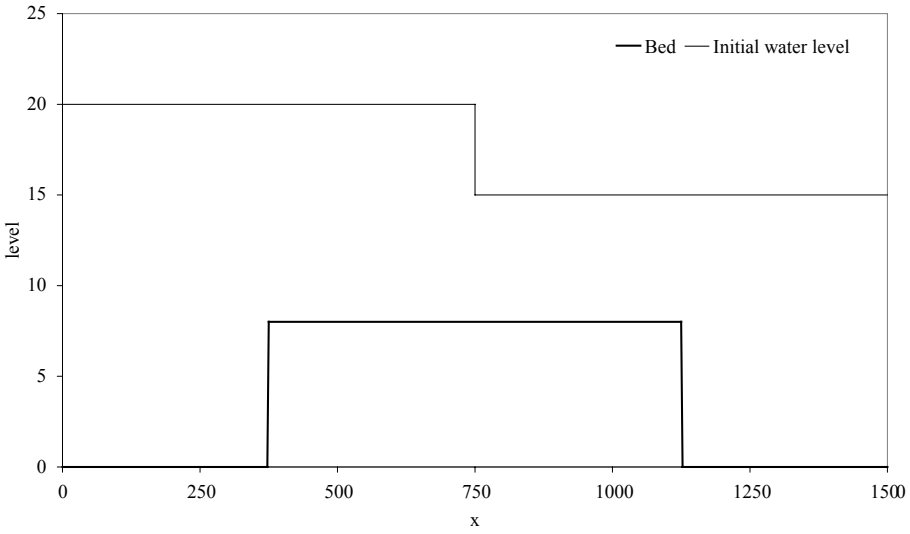

Fig. 7. The initial water level in the test problem 5.1.4.

The computations are performed with the space step $\Delta x = 0.25$ m and by using $c_{\mathrm{CFL}} = 0.9$. The Manning friction factor is set to 0.0125 over the whole numerical domain. Since in both considered cases the water propagates over the dry bed an appropriate numerical treatment of wetting/drying front should be included in computations. This is done according to [3].

In Figs. 10 and 11, we compare the numerical results obtained with the finite volume WENO scheme with the experimental results and with the first-order Roe scheme. The water depth evolutions at different measurement points are presented. Positions of the measurement points are given in Table 5. From the presented figures we can conclude that some improvements are obtained when the higher-order schemes are used. The global trend of the numerical solutions is similar in both numerical cases, but there are few positions where the higher-order scheme becomes closer to the experimental data. The large deviations that arise in some measurement points are probably the consequence of some real water flow effects that are not completely modelled by the the shallow water equations, such as energy dissipation for example. We must emphasize ones again that without balancing of the schemes that is developed in the paper, the finite volume WENO schemes would be unusable for implementation in the presented problems.

5.1.6. Test problem with discontinuous riverbed

We consider now an academical test example with the discontinuous riverbed given by the step function

$$z(x) = \begin{cases} 1, & x < 0, \\ 0, & x > 0. \end{cases} \tag{73}$$

The initial conditions are defined with

$$h(x,0) = \begin{cases} 1, & x < 0, \\ 0.6527036446614, & x > 0 \end{cases} \quad \text{and} \quad hv(x,0) = \sqrt{2g}, \tag{74}$$

where $g = 9.81$. In the case of the stationary flow with constant discharge, the given initial conditions should remain unchanged. When we apply our schemes to this problem, we noticed that they produce some consistency error in water depth on the right side of the discontinuity, which is independent of the cell sizes.

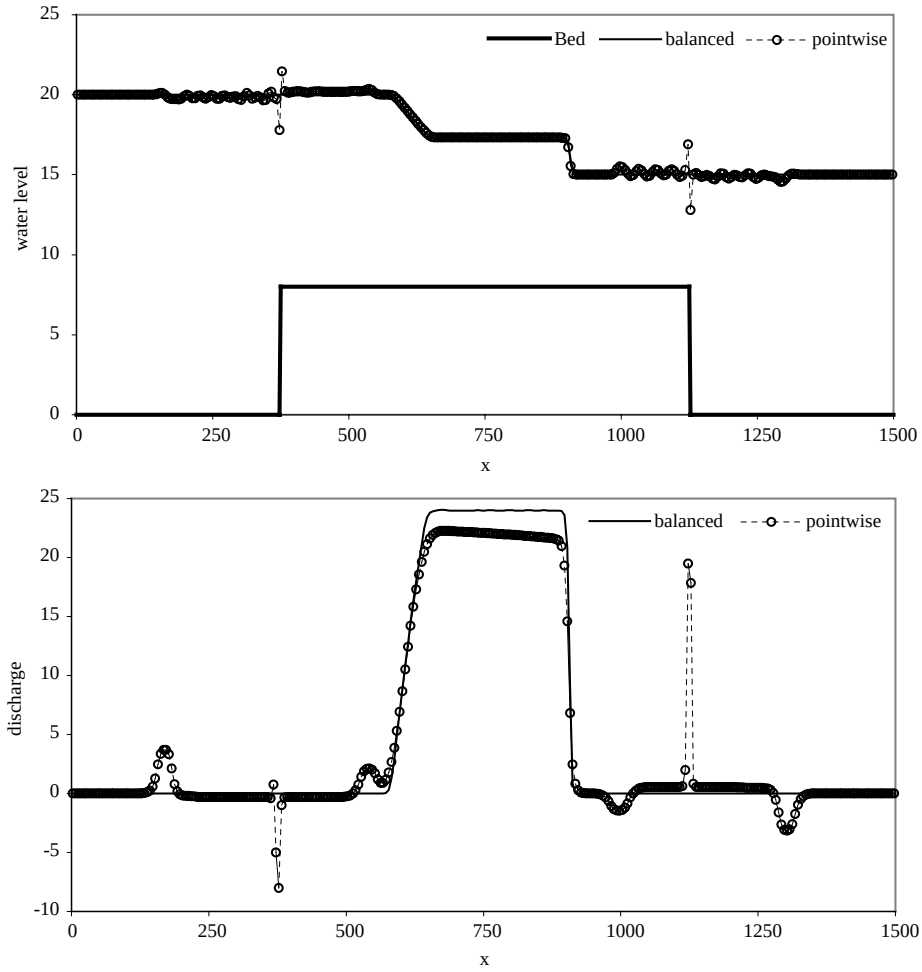

Fig. 8. The comparison of the central WENO schemes, $r = 5$ (test problem 5.1.4). Top: water level at $t = 15$ s; Bottom: discharge at $t = 15$ s.

The same phenomenon is observed when the first-order scheme introduced in [2] is applied. The finite volume WENO schemes in combination with the HLL Riemann solver (see [33]) produces the similar error also, and the same is true for the finite difference WENO schemes. In Table 6, where we present the numerically obtained values of the water depth on the right of the discontinuity, the consistency errors that arise can be nicely observed. Since the considered numerical schemes approximate the shallow water equations that are not valid in the region where the discontinuity in the riverbed is present, we cannot expect from these schemes to give a correct results. Actually, we think the approximate Riemann solvers that are used, fail in such cases. Since the considered WENO schemes are used in combination with the standard approximate Riemann solvers, we cannot expect the consistency error to disappear. However, there exists some ways to correct the schemes locally near the position of the discontinuity. Particularly, following the ideas presented in [34], where the surface gradient method is extended to treat correctly the flow over vertical step, some modifications of the approximate Riemann solvers at the positions of the discontinuity of the riverbed should be done. Since a detail analysis of this theme could be very extensive, it goes beyond the scope of this paper.

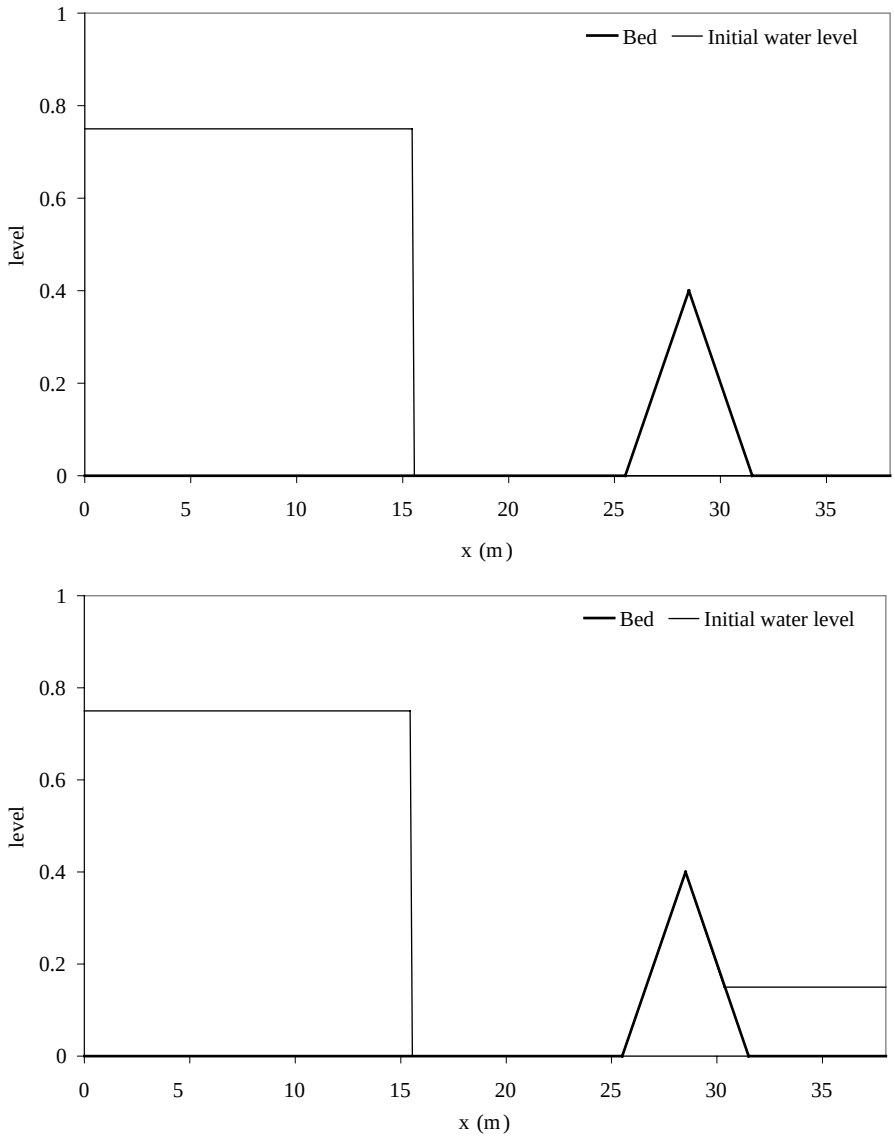

Fig. 9. The initial water level in the test problem 5.1.5. Top: the case with the completely dry channel; Bottom: the case with the partially wet channel.

5.2. Open-channel flow equations

5.2.1. Tidal wave propagation in a channel proposed by Working Group on Dam-Break Modelling

When we consider the open-channel flow equations the typical test problem to check the numerical scheme is the test proposed by Working Group on Dam-Break Modelling [13]. The channel is rectangular with variable bed and width as defined in [2] and presented in Fig. 12. Contractions and expansions of the considered channel cause that additional forces appear, hence the additional balancing requirements arise, as we have seen when the application of the numerical schemes to the open-channel flow was considered.

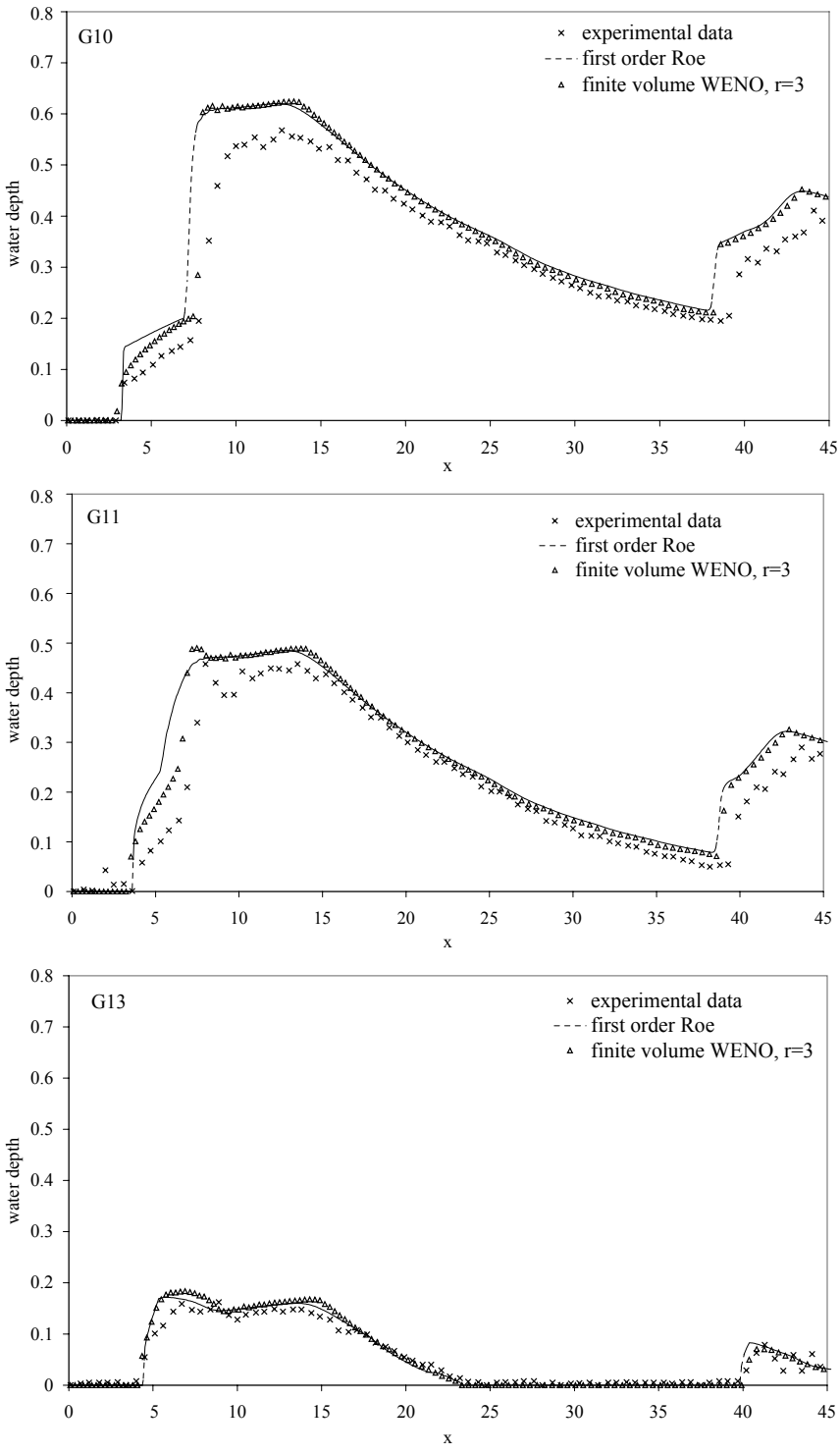

Fig. 10. Water depth at the measurement points G10, G11 and G13. Comparison of the numerical results and the experimental data in the version of the test problem 5.1.5. with the dry bed.

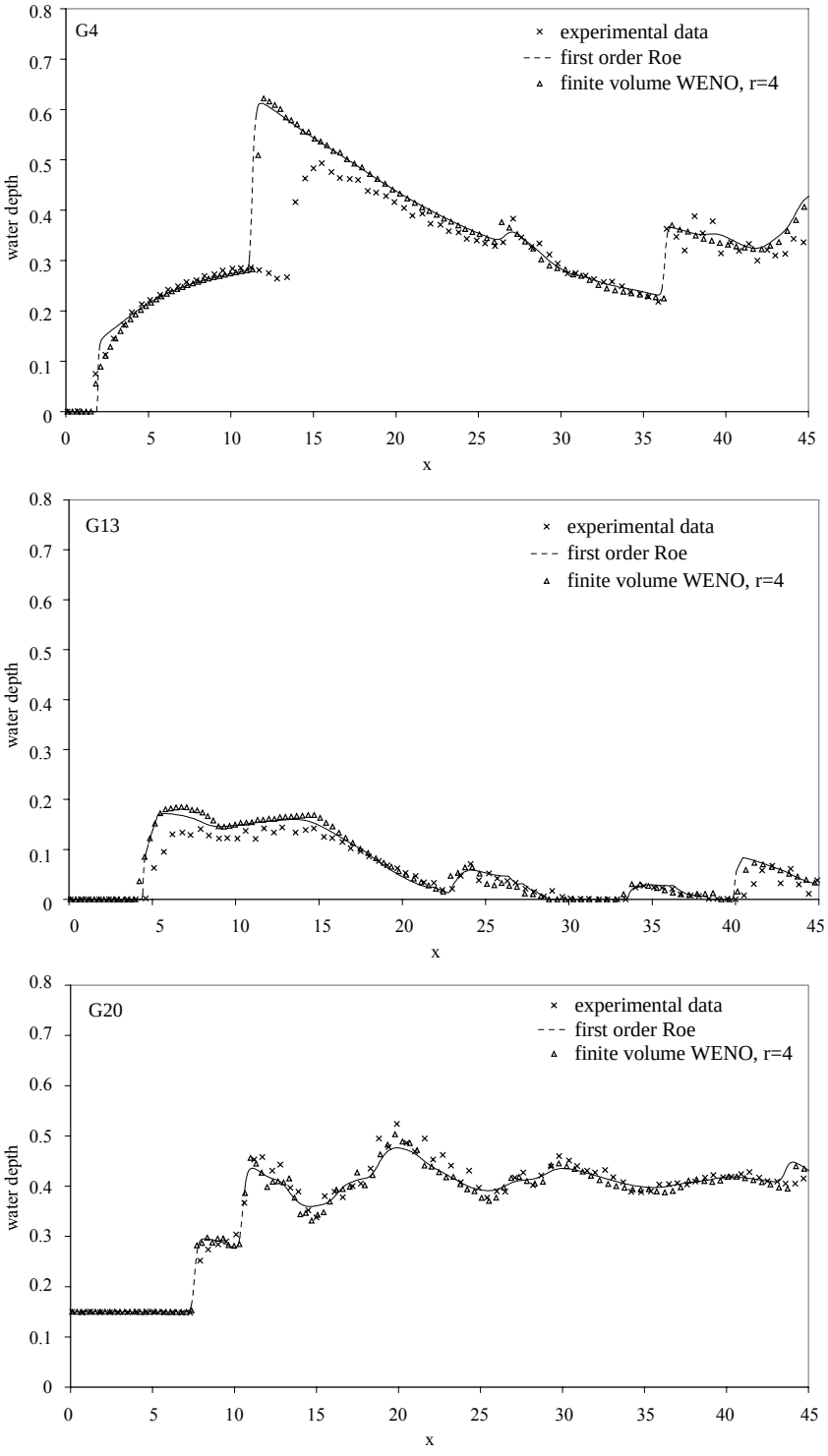

Fig. 11. Water depth at the measurement points G4, G13 and G20. Comparison of the numerical results and the experimental data in the version of the test problem 5.1.5. with the wet bed.

Table 5
Positions of the measurement points (test problem 5.1.5.)

Measurement point	G4	G10	G11	G13	G20
Position $x(m)$	19.5	25.5	26.5	28.5	35.5

Table 6
Water depths on the right side of the discontinuity obtained with different numerical schemes (test problem 5.1.6.)

Numerical method	h
First-order Roe	0.638086760619
Second-order flux limited	0.638086760619
Finite volume WENO with Roe solver	0.642073632474
Finite volume WENO with HLL solver	0.690837958716
Finite difference WENO Roe	0.642073632474
Finite difference WENO locally Lax-Friedrichs	0.638725676769

Thus, it is interesting to check the behaviour of the balanced numerical scheme in that type of channel. We suppose now that the tidal wave is incoming from the left channel boundary. It is defined with

$$h(0,t) = 16.0 - 4.0\sin\left[\pi\left(\frac{4t}{86,400} + \frac{1}{2}\right)\right], \tag{75}$$

while the right boundary condition is

$$v(1500,t) = 0. \tag{76}$$

Eq. (75) simulates a tidal wave of 4 m amplitude and the period of $t = 21,600$ s. The water is initially at rest with the water level equal 12 m. The computations are performed with space step $\Delta x = 2.5$ m and with CFL coefficient $c_{\mathrm{CFL}} = 0.7$.

We give numerical results after $t = 10,800$ s obtained by the central WENO scheme with $r = 3$. Results presented in Fig. 13, where the comparison between the balanced and the nonbalanced versions of the scheme is made, clearly illustrate the superiority of the balanced schemes. As we expect

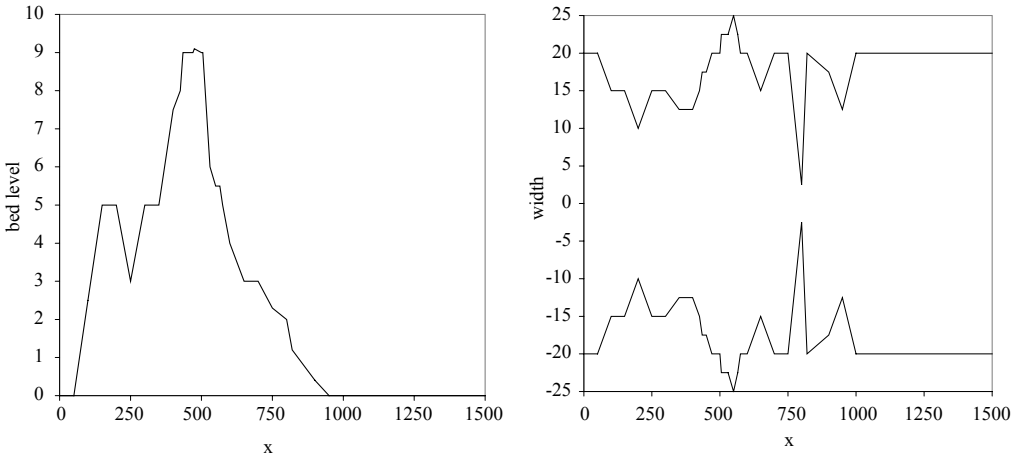

Fig. 12. Test problem 5.2.1. Left: bed level; Right: width of the channel.

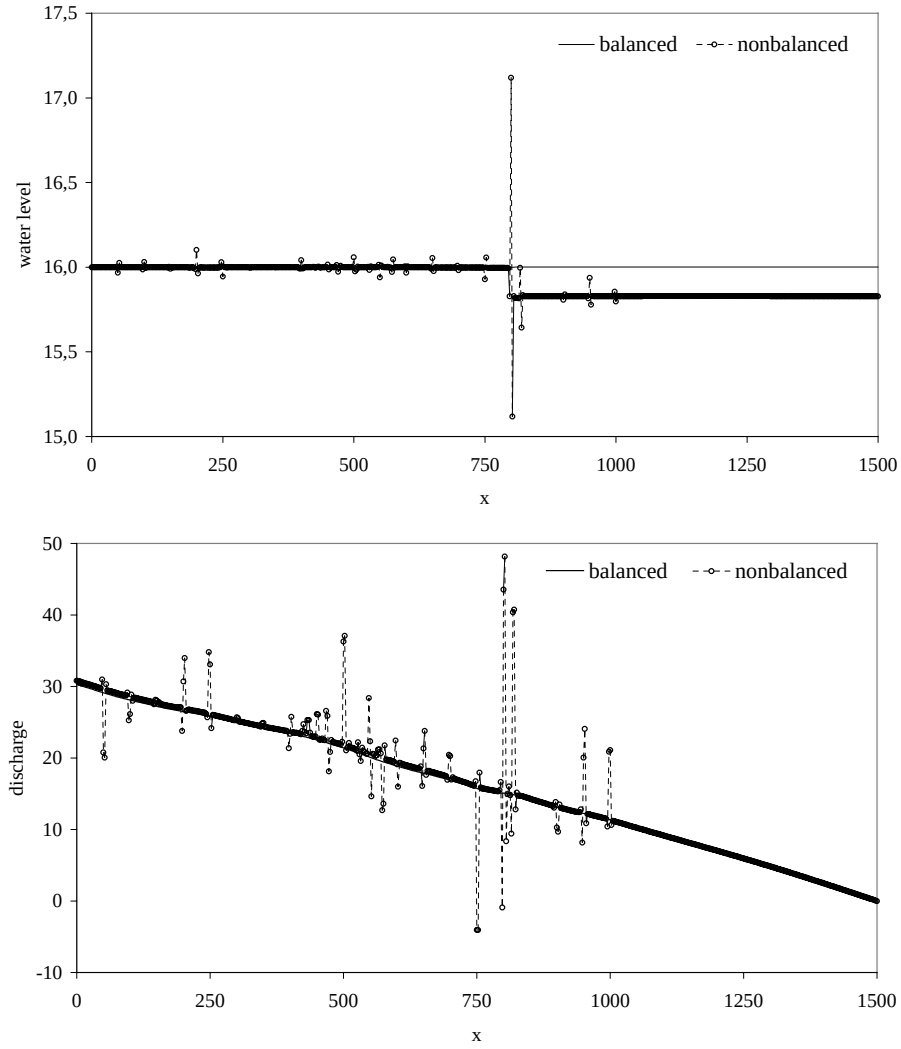

Fig. 13. The comparison of the central WENO scheme, $r = 3$ (test problem 5.2.1). Top: water level at $t = 10,800$ s; Bottom: discharge at $t = 10,800$ s.

the results obtained with the finite volume WENO schemes shows the same trend, i.e., the results obtained with the balanced scheme are very accurate, while when the pointwise scheme is used large errors appear. However, according to Vázquez-Cendón [28], we can evaluate the asymptotically exact solution and verify the proposed numerical schemes by comparing the numerically obtained results with it. Since the agreement with the exact solution is very well for all the balanced WENO schemes, we omit to show this comparison.

5.2.2. Steady flow in a channel with variable height and width

This is an example for testing the efficiency of the presented numerical schemes when the steady-state solutions in a channel with variable height and width are considered. The geometry for this test problem is taken from [9]. The channel height and width are defined over the interval [0,3] with

$$z(x) = \begin{cases} 0.1\cos^2(\pi(x-1.5)) & \text{if } |x-1.5| < 0.5, \\ 0 & \text{otherwise} \end{cases} \tag{77}$$

and

$$B(x) = \begin{cases} 1 - 0.1\cos^2(\pi(x-1.5)) & \text{if } |x-1.5| < 0.5, \\ 0 & \text{otherwise} \end{cases} \tag{78}$$

(see Fig. 14).

First we consider the steady state obtained by imposing the constant discharge of 0.1 m^3/s at the upstream boundary and the water depth of 1 m on the downstream boundary. The imposed conditions cause the purely subcritical flow over the whole domain, which could be evaluated analytically. Since for the given case the balanced numerical schemes presented in the paper produce very accurate results that are almost indistinguishable from the analytical solution, we decide to show just the comparison of the numerical solutions obtained with the balanced and the nonbalanced version of the central WENO scheme with $r = 5$. However, in Fig. 15 we present also the analytical solution. While the results obtained with the balanced numerical scheme are coincident with the analytical solution, the nonbalanced version produces the numerical oscillations that are a consequence of transformations between the staggered and the nonstaggered mesh which do not respect balancing of the flux gradient and the source term.

In the given channel we consider now the case defined with the discharge equal 1.88 m^3/s on the upstream boundary and the water depth of 1 m on the downstream boundary. Due to the variable bed and width of the channel, and the imposed discharge the flow becomes supercritical at the point of maximum contraction and maximum height, and then returns back to the subcritical. Therefore, at the critical point, a hydraulic jump arises. In Fig. 16, we compare the finite volume WENO and the central WENO scheme with the analytical solution. The position and the strength of the jump is predicted accurately with both the numerical schemes. However, when the solution obtained with the finite volume WENO scheme is considered, their high resolution properties are revealed. As for all the known numerical schemes, a consistency error in the discharge occurs at the place of jump for both numerical schemes. However, when the finite volume WENO scheme is used there is just one point in which such an error arises, while when the central WENO scheme is used, the error is greater and spread over few points. We explain this phenomenon by the fact that

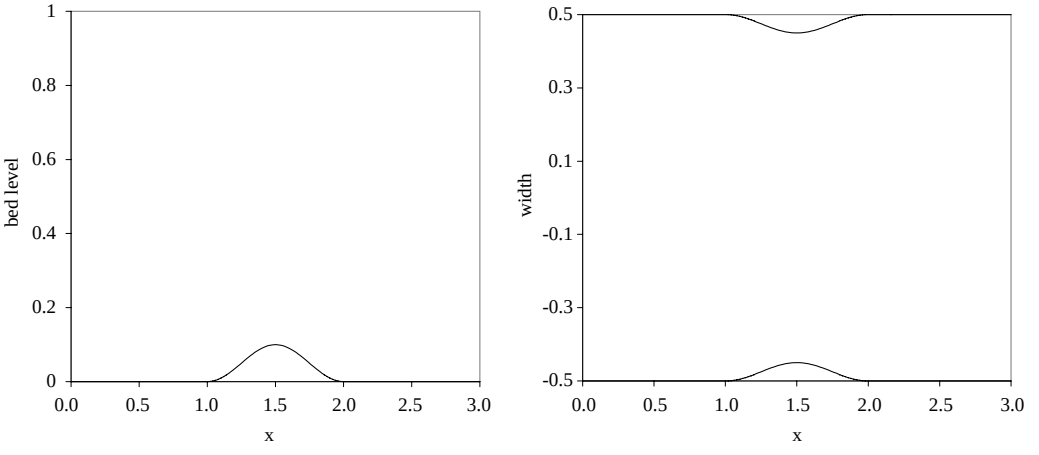

Fig. 14. Test problem 5.2.2. Left: bed level; Right: width of the channel.

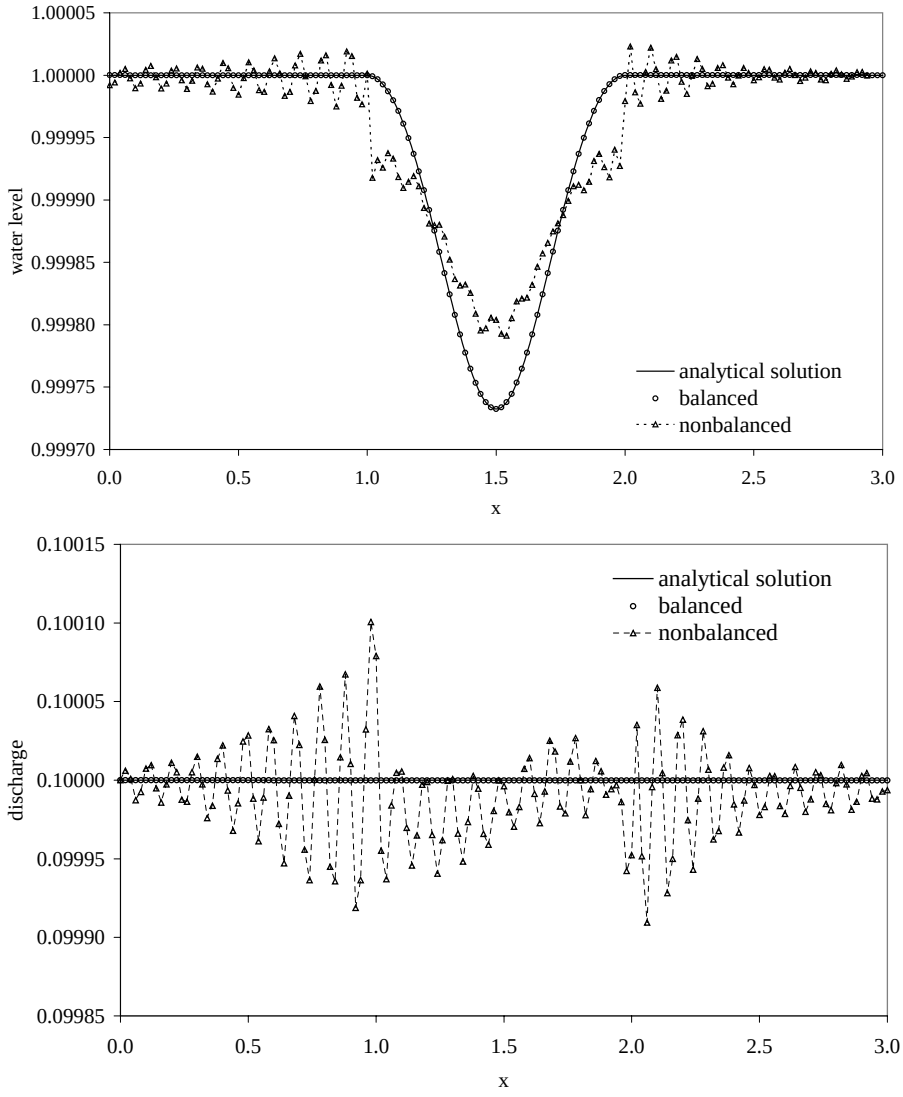

Fig. 15. The comparison of the central WENO scheme, $r = 5$ (test problem 5.2.2). Top: water level; Bottom: discharge.

averaging over the staggered and the nonstaggered mesh spread out the numerical disturbance over the domain.

In the similar test example for the shallow water equations (test problem 5.1.3), we compare our WENO schemes with the second-order flux limited scheme. Since the numerical solutions computed with all the balanced schemes developed in the paper are in this test very close to the numerical solutions obtained with the first-order Roe and the second order flux limited scheme, which are both in the steady-state case at least second-order accurate, the presentation of the results and the further analysis is omitted here.

5.2.3. Water wave propagation through a natural watercourse

We consider the test problem on a natural watercourse of the southern part of the river Gacka (Croatia) [26]. We take part of the channel about 2400 m long, with very varying cross-sections (see Fig. 17). The

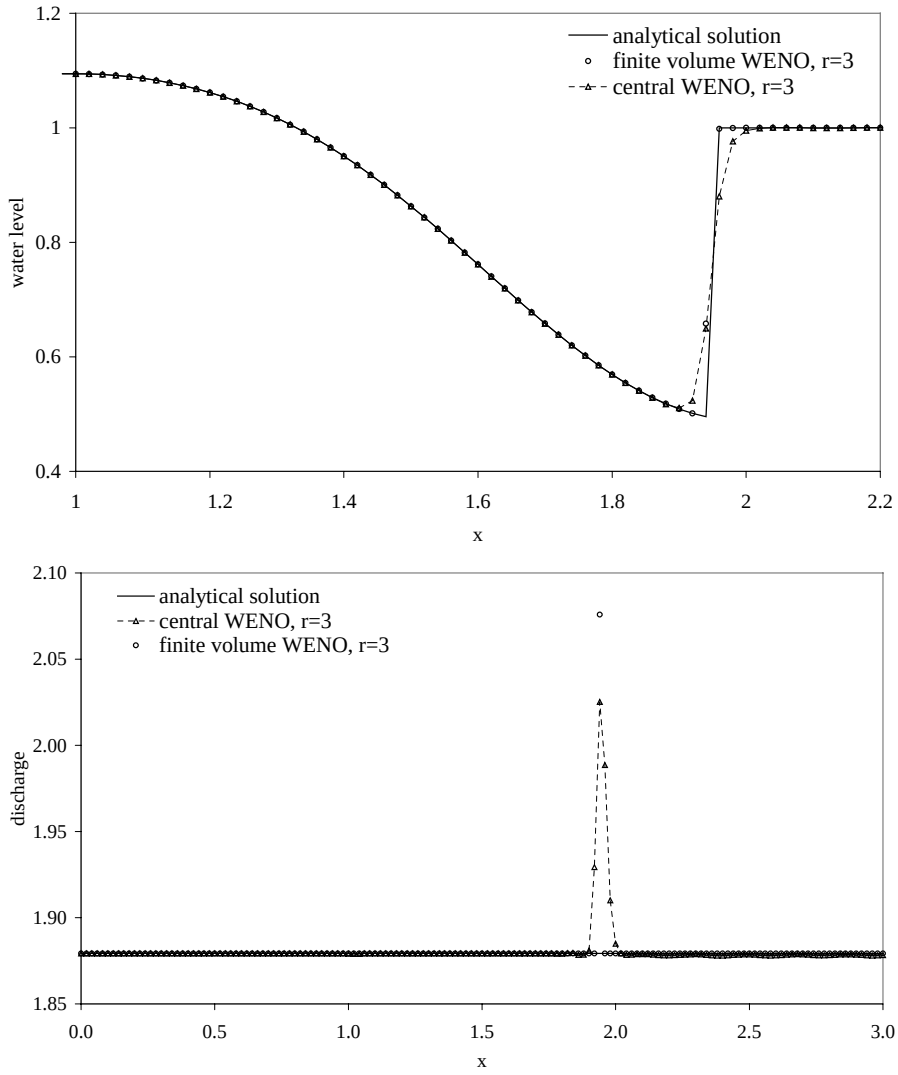

Fig. 16. Comparison of the numerical schemes and analytical solution. Steady hydraulic jump in the test problem 5.2.2. Top: water level; Bottom: discharge.

friction forces are included in the computations. Depending on the properties of the channel the Manning's friction factor values vary between 0.03 and 0.05. Our goal is to compute a steady-state solution based on the boundary conditions we set. On the inflow boundary the constant discharge of 20 m^3/s is imposed, while on the outflow we assume the normal flow arises. The discharge associated to it can be computed from the relation $Q = S_0^{1/2} A^2 R^{2/3}/M$. Here, S_0 denotes the bottom slope. All the values in the above relation must be evaluated at the outflow boundary profile. The same test problem is considered in [30], where the flow is evaluated by using the balanced second-order flux limited scheme.

The steady-state solution is computed with the finite volume WENO scheme with $r = 3$. The mesh size is taken $\Delta x = 10$ m, while the CFL coefficient is set to 0.9. In order to show that the considered scheme solve well the situations where the dry domain appear, we start with the initially dry channel. Like in the test

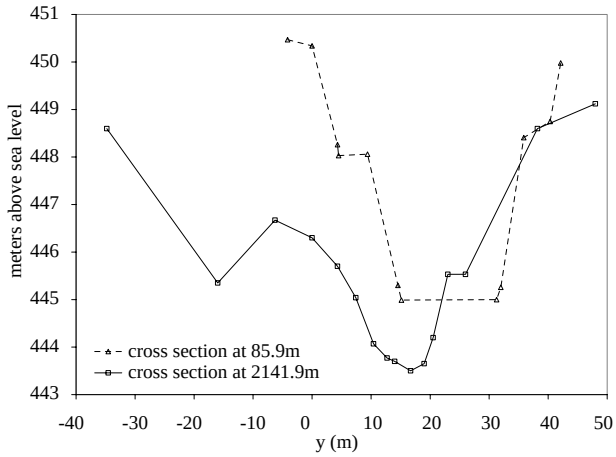

Fig. 17. Two cross-sections in the natural watercourse (test problem 5.2.3) (y-distance along the cross-section).

problem 5.1.5, for the numerical treatment of the wetting front advance over a dry bed we use the technique presented in [3]. The solution obtained after three hours of the water wave propagation we refer as the steady-state solution. In Fig. 18, we present the water wave propagation until the steady-state water level is reached. The shown results are obtained with the balanced scheme. The comparison between the pointwise and the balanced version of the scheme at the steady state is then presented Fig. 19. The errors in the discharge computed with the pointwise source term evaluation are unacceptable large. It is true that errors also arise when the balanced scheme is used, but they are of much lower order then the errors obtained by the pointwise scheme.

What we must emphasize is, that in combination with the pointwise evaluation of the friction term, the CFL coefficient had to be reduced to 0.5, while here, with the semi-implicit discretization [4] it is set to 0.9. With that, the statement that the semi-implicit discretization reinforces the CFL condition is confirmed.

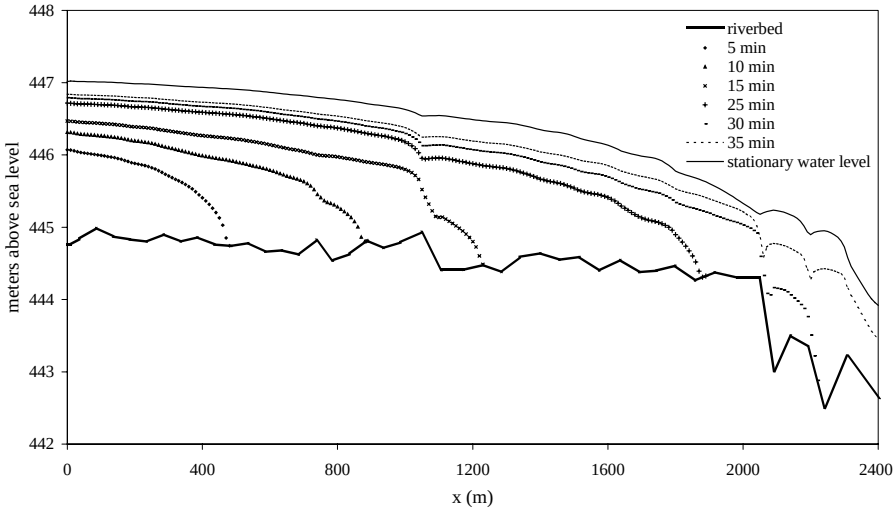

Fig. 18. Water wave propagation in the test problem 5.2.3 obtained with the finite volume WENO scheme, $r = 3$.

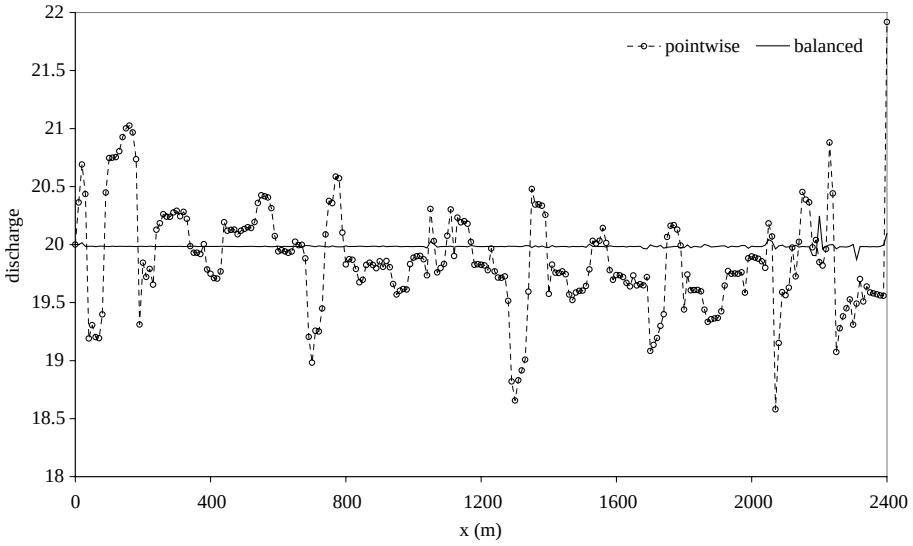

Fig. 19. The comparison of the finite volume WENO scheme, $r = 3$. Discharge at the steady state in the test problem 5.2.3.

6. Concluding remarks

After we extended the finite difference WENO schemes to the balance laws in [29], in this work we do the same for the finite volume WENO schemes and the nonstaggered central WENO schemes also. With the extension of the finite volume WENO schemes we obtain the balanced higher-order numerical schemes for balance laws that can be applied to the nonuniform meshes also. There are two types of the balance laws that we consider here: the shallow water equations and the open-channel flow equations. Both laws contain a geometrical source term and the second law additionally includes spatially varied flux function. Thus, when the Roe approximate Riemann solver is used in the finite volume WENO scheme the spatial part of the flux is taken into account. Furthermore, the source term should be appropriately discretized. Such an assumed general formulation, in combination with the appropriate definitions of the terms that depend on the particular balance law, leads to the balanced finite volume WENO schemes. On the other hand, the central WENO schemes modification for balance laws consists of three parts. First, we obtain the balancing in the predictor and also in the corrector step of the scheme. In addition, we perform the procedure of passing from the nonstaggered mesh to the staggered one and then after the time step is performed return back to the nonstaggered, according to the idea of preserving the quiescent flow steady state. In the open-channel flow case we obtained the balanced central WENO schemes only for the rectangular cross-section channels, while no restriction is needed for the finite volume WENO schemes.

The numerical results in the last section confirm the necessity of using the balanced schemes, especially for the cases where the channels with highly irregular geometry arise. Moreover, the accuracy test results show that the order of accuracy of the new schemes is not deteriorated with the proposed reformulations, when compared with the classical versions. Also the CPU times measured for both proposed types of the schemes show satisfying results.

References

[1] D.S. Bale, R.J. LeVeque, S. Mitran, J.A. Rossmanith, A wave propagation method for conservation laws and balance laws with spatially varying flux functions, SIAM J. Sci. Comput. 24 (3) (2003) 955.

[2] A. Bermùdez, M.E. Vázquez, Upwind methods for hyperbolic conservation laws with source terms, Comput. Fluids 23 (8) (1994) 1049.
[3] P. Brufau, M.E. Vázquez-Cendón, P. García-Navarro, A numerical model for flooding and drying of irregular domains, Int. J. Numer. Methods Fluids 39 (2002) 247.
[4] J. Burguete, P. García-Navarro, Efficient construction of high-resolution TVD conservative schemes for equations with source terms: application to shallow-water flows, Int. J. Numer. Methods Fluids 37 (2001) 209.
[5] T. Chacón Rebollo, A. Domínguez Delgado, E.D. Fernández Nieto, A family of stable numerical solvers for the shallow water equations with source terms, Comput. Methods Appl. Mech. Engrg. 192 (2003) 203.
[6] T. Chacón Rebollo, A. Domínguez Delgado, E.D. Fernández Nieto, An entropy-correction free solver for non-homogeneous shallow water equations, Math. Model. Numer. Anal., M2AN 37 (3) (2003) 363.
[7] N. Črnjarić-Žic, S. Vuković, L. Sopta, Extension of ENO and WENO schemes to one-dimensional sediment transport equations, Comput. Fluids 33 (1) (2004) 31.
[8] A. Harten, B. Engquist, S. Osher, S.R. Chakravarthy, Uniformly high order accurate essentially non-oscillatory schemes III, J. Comput. Phys. 71 (1987) 231.
[9] M.E. Hubbard, P. García-Navarro, Flux difference splitting and the balancing of source terms and flux gradient, J. Comput. Phys. 165 (2000) 89.
[10] T. Gallouët, J.-M. Hérard, N. Seguin, Some approximate Godunov schemes to compute shallow water equations with topography, Comput. Fluids 32 (2003) 479.
[11] P. García-Navarro, M.E. Vázquez-Cendon, On numerical treatment of the source terms in the shallow water equations, Comput. Fluids 29 (2000) 951.
[12] L. Gosse, A well-balanced scheme using non-conservative products designed for hyperbolic systems of conservation laws with source terms, Math. Mod. Meth. Appl. Sci. 11 (2001) 339.
[13] P. Goutal, F. Maurel, Proceedings of the 2nd Workshop on Dam-Break Wave Simulation, Technical Report HE-43/97/016A, Electricité de France, Département Laboratoire National d'Hydraulique, Groupe Hydraulique Fluviale, 1997.
[14] J.-M. Greenberg, A.-Y. LeRoux, A well-balanced scheme for the numerical processing of source terms in hyperbolic equation, SIAM J. Numer. Anal. 33 (1) (1996) 1.
[15] G.-S. Jiang, D. Levy, C.-T. Lin, S. Osher, E. Tadmor, High-resolution nonoscillatory central schemes with nonstaggered grids for hyperbolic conservation laws, SIAM J. Numer. Anal. 35 (6) (1998) 2147.
[16] A. Kurganov, D. Levy, Central-upwind schemes for the Saint–Venant system, Math. Model. Numer. Anal., M2AN 36 (3) (2002) 397.
[17] A. Kurganov, E. Tadmor, New high-resolution central schemes for nonlinear conservation laws and convection–diffusion equations, J. Comput. Phys. 160 (2002) 241.
[18] R.J. LeVeque, Balancing source terms and flux gradients in high-resolution Godunov methods: the quasi-steady wave propagation algorithm, J. Comput. Phys. 146 (1998) 346.
[19] R.J. LeVeque, Finite Volume Methods for Hyperbolic Problems, Cambridge University Press, 2002.
[20] D. Levy, G. Puppo, G. Russo, Central WENO schemes for hyperbolic systems of conservation laws, Math. Model. Numer. Anal. 33 (1999) 547.
[21] S.F. Liotta, V. Romano, G. Russo, Central schemes for balance laws of relaxation type, SIAM J. Numer. Anal. 38 (4) (2000) 1337.
[22] X.-D. Liu, S. Osher, T. Chan, Weighted essentially non-oscillatory schemes, J. Comput. Phys. 115 (1994) 200.
[23] J. Qiu, C.-W. Shu, On the construction comparison, and local characteristic decomposition for high order central WENO schemes, J. Comput. Phys. 183 (2002) 187.
[24] C.-W. Shu, Essentially non-oscillatory and weighted essentially non-oscillatory schemes for hyperbolic conservation laws, in: B. Cockburn, C. Johnson, C.-W. Shu, E. Tadmor (Eds.), Advanced Numerical Approximation of Nonlinear Hyperbolic Equations, Lecture Notes in Mathematics, vol. 160, Springer, Berlin/New York, 1998, p. 325.
[25] C.-W. Shu, S. Osher, Efficient implementation of essentially non-oscillatory shock capturing schemes II, J. Comput. Phys. 83 (1989) 32.
[26] L. Sopta, S. Vuković, L. Kranjčević, Mathematical model of water wave propagation in the southern part of river Gacka, Technical Report for Hydroelectric power-plant 'Senj', Rijeka (Croatia), 1999. Available from: http://www.riteh.hr/zav_katd_sluz/zav_meh_flu_rac_inz/katedre/rac_inz/research.htm.
[27] K. Xu, A well-balanced gas-kinetic scheme for the shallow water equations with source terms, J. Comput. Phys. 178 (2000) 533.
[28] M.E. Vázquez-Cendón, Improved treatment of source terms in upwind schemes for the shallow water equations in channel with irregular geometry, J. Comput. Phys. 148 (1999) 497.
[29] S. Vuković, L. Sopta, ENO and WENO schemes with the exact conservation property for one-dimensional shallow water equations, J. Comput. Phys. 179 (2002) 593.
[30] S. Vuković, L. Sopta, Upwind schemes with exact conservation property for one-dimensional open channel flow equations, SIAM J. Sci. Comput. 24 (5) (2003) 1630.

[31] S. Vuković, N. Črnjarić-Žic, L. Sopta, WENO schemes for balance laws with spatially varying flux, J. Comput. Phys. (2004), in press.
[32] M. Zhang, C.-W. Shu, C.K. Wong, S.C. Wong, A weighted essentially non-oscillatory numerical scheme for a multi-class Lighthill–Whitham–Richards traffic flow model, J. Comput. Phys. 191 (2003) 639.
[33] J.G. Zhou, D.M. Causon, C.G. Mingham, D.M. Ingram, The surface gradient method for the treatment of source terms in the shallow-water equations, J. Comput. Phys. 168 (2001) 1.
[34] J.G. Zhou, D.M. Causon, D.M. Ingram, C.G. Mingham, Numerical solutions of the shallow water equations with discontinuous bed topography, Int. J. Numer. Methods Fluids 38 (2002) 769.